Slab mantle dehydrates beneath Kamchatka – yet recycles water into the deep mantle

Matthias Konrad-Schmolke[1,2,*], Ralf Halama[1,3], Vlad C. Manea[4]

[1] Institute of Earth and Environmental Science, University of Potsdam, Karl-Liebknecht-Str. 24-25, 14476 Potsdam, Germany

[2] Department of Earth Sciences, University of Gothenburg

[3] School of Physical and Geographical Sciences, University of Keele, Keele, Staffordshire, ST5 5BG, United Kingdom

[4] Computational Geodynamics Laboratory, Geosciences Centre, Universidad Nacional Autónoma de México, Juriquilla, Mexico

* Corresponding author:
Matthias Konrad-Schmolke
University of Gothenburg
Department of Earth Science
Guldhedsgatan 5a
40530 Gothenburg
E-mail: mks@gvc.gu.se
Tel: +46-729-275615

Author Contributions: MKS designed the thermodynamic-geochemical model and VM developed the thermal model. MKS and RH wrote the manuscript, and all authors participated in the discussion.

Submitted March 2016

Abstract

The subduction of hydrated slab mantle is the most important and yet weakly constrained factor in the quantification of the Earth's deep geologic water cycle. The most critical unknowns are the initial hydration state and the dehydration behavior of the subducted oceanic mantle. Here we present a combined thermomechanical, thermodynamic and geochemical model of the Kamchatka subduction zone that indicates significant dehydration of subducted slab mantle beneath Kamchatka.

Evidence for the subduction of hydrated oceanic mantle comes from across-arc trends of boron concentrations and isotopic compositions in arc volcanic rocks. Our thermodynamic-geochemical models successfully predict the complex geochemical patterns and the spatial distribution of arc volcanoes in Kamchatka assuming the subduction of hydrated oceanic mantle. Our results show that water content and dehydration behavior of the slab mantle beneath Kamchatka can be directly linked to compositional features in arc volcanic rocks.

Depending on hydration depth of the slab mantle, our models yield water recycling rates between 1.1 x 10^3 and 7.4 x 10^3 $TgMa^{-1}km^{-1}$ corresponding to values between 0.75 x 10^6 and 5.2 x 10^6 $TgMa^{-1}$ for the entire Kamchatkan subduction zone. These values are up to one order of magnitude lower than previous estimates for Kamchatka (Hacker 2008; Van Keken et al., 2011), but clearly show that subducted hydrated slab mantle significantly contributes to the water budget in the Kamchatkan subduction zone.

Introduction

The amount and distribution of the Earth's water is a so far unresolved problem despite its importance for geodynamics, atmosphere and biosphere. The silicate Earth's total water content is in the order of 2700 ± 1350 ppm(wt) (Marty 2012), whereas hydrosphere and atmosphere represent only 250 ppm water relative to the Earth's total mass. It is, indeed, the Earth's mantle that is thought to represent by far the Earth's largest water reservoir. Water in nominally anhydrous minerals (NAM) and in dense hydrous magnesium silicates (DHMS) can make up ten times of the water that is stored in the oceans at the Earth's surface (Smyth et al., 2006, Angel et al., 2001; Frost 1999; Ohtani et al., 2001). Recent findings of ringwoodite highlighted the hydrous nature of the mantle transition zone and hence point to the importance of the mantle regarding the quantification of the Earth's water budget (Pearson et al., 2014).

Two competing processes are crucial for the distribution of water between the Earth's hydrosphere and the silicate mantle: (1) outgassing of water from the mantle through volcanism and (2) subduction of hydrated oceanic lithosphere that enables recycling of water from the hydrosphere into the deeper mantle. The interplay of these opposing processes displays a dynamic equilibrium that controls the distribution of water between the Earth's surface and the deeper mantle (Rüpke et al., 2004, Hacker 2008, van Keken et al., 2011; Freundt et al., 2014). Both of these processes are closely related to the Earth's internal thermal structure as geodynamic processes, such as mantle convection and plate motion, are primarily heat dependent. It is evident that continuous cooling of our planet has significantly changed geodynamics on Earth since the Early Archean (Brown 2008; Stern 2008; Condie and Kröner, 2008). Hence, subducting plates become cooler, hydrous phases therein become more stable and larger amounts of water can be dragged down to the deep mantle (e.g., Maruyama and Okamoto 2007).

This increasingly important process will potentially shift the distribution of water between the Earth's surface and the silicate mantle in the future.

Advances in computational capabilities nowadays allow numerical modelling of water cycling in subduction zones based on thermodynamic and thermo-mechanical models (Rüpke et al., 2004; Hacker 2008; Van Keken et al., 2011, Konrad-Schmolke and Halama 2014). Balancing the amount of water brought into the subduction zone by the hydrated oceanic lithosphere with the modeled dehydration reactions in the subducting slab enables a quantitative estimation of how much water is subducted beyond the volcanic arcs in subduction zones (e.g., Hacker 2008; van Keken et al., 2011). However, the results of these numerical models differ significantly in the intensity of water recycling into the mantle, such that estimates of the total overturning times of the entire hydrosphere range from 1.6 to 3.3 Ga depending on the model input parameters.

All of the numerical models show that the hydration state of the subducted mantle lithosphere is the major factor in water recycling in subduction zones, as the amount of water potentially present in hydrated sub-oceanic serpentinites is several times larger than in the altered oceanic crust (AOC). Further, due to the specific thermal structure in subducting plates – involving a thermal minimum extending sub-parallel to the plate surface at slab mantle depth – dehydration reactions in the slab mantle can be inhibited and water contained therein can be directly transferred into DHMS (e.g. Phase A). Within such dense hydrous phases water can be subducted as deep as the mantle transition zone between 410 and 660 km depth and once brought to this depth, the stability of wadsleyite and ringwoodite enables storage of water in the order of several hydrosphere masses (e.g. Karato, 2011; Jacobsen and van der Lee, 2006; Pearson et al., 2014).

Numerical simulations of the water budget in subduction zones strongly depend on the setting of the critical model parameters, most of which are poorly constrained (Rüpke et al., 2006). Hence, unambiguous information on the subducted water amount and the global water cycle is difficult to extract from numerical models alone without further external information. Surface expressions of the dehydration reactions in the slab, such as the chemical composition of arc lavas, are commonly the only reliable proxies for the water budget in deeply subducted rocks (e.g., Pearce and Peate 1995; Ryan et al., 1995; Hebert et al., 2009; Kimura et al., 2009). Based on this assumption Rüpke et al. (2002) and Walowski et al. (2015) presented thermodynamic-geochemical models of the Nicaragua and Cascadia subduction zones, respectively, the results of which indicate a significant contribution of dehydration reactions in the subducted oceanic mantle on arc lava chemistry. In both cases the structural position as well as the chemical imprint on arc lavas clearly point towards water release from the downgoing slab mantle thus indicating that the subducted mantle lithosphere in these subduction zones is indeed hydrated to significant extents. Both works further show the capacity of thermodynamic-geochemical models to discriminate fluid sources in subducting slabs based on characteristic across-arc variations in arc lava chemistry.

In this paper we model the dehydration of the oceanic lithosphere in the Kamchatkan subduction zone utilizing two-dimensional thermodynamic models based on Gibbs energy minimization. Dehydration reactions, fluid liberation, fluid migration and fluid-rock interaction are modeled based on a thermal pattern derived from thermo-mechanical finite element models of three profiles across the Kamchatkan subduction zone. The results of the thermodynamic models are then used to simulate boron release from the slab, which is compared to the observed variations in the erupted lavas in Kamchatka. Our results indicate that for Kamchatka, slab mantle dehydration is likely a major process for the formation of some arc volcanoes and that water retained in the slab mantle can potentially be transported beyond the volcanic arc.

Geological setting of the Kamchatka subduction zone

The Kamchatka subduction zone (Fig. 1) is one of the most volcanically active regions on Earth (e.g., Portnyagin and Manea 2008). It comprises three distinct volcanic chains – the Eastern Volcanic Front (EVF), the volcanoes in the Central Kamchatkan Depression (CKD) and the Sredinny Range (SR) – for which detailed geochemical and B isotope data have been published (e.g., Ishikawa et al., 2001; Churikova et al., 2001; Portnyagin et al., 2007). Furthermore, geophysical studies yielded detailed insight into the shape and dip of the subducted plate as well as the crust and mantle structure beneath Kamchatka (e.g. Manea and Manea, 2007; Levin et al., 2002).

The Kamchatka peninsula is part of the Kurile-Kamchatka arc where the Pacific plate is subducted northwestward since the Late Cretaceous to Early Paleocene (e.g., Avdeiko et al., 2007). Subduction and differential counterclockwise slab rollback have led to the formation of the Kurile backarc basin, the Hokkaido-Sachalin dextral strike slip system and the Ochotsk sea (Schellart et al., 2003). Accretion and amalgamation of different volcanic arcs in the northern part of the subduction zone have led to the formation of the Kamchatkan peninsula as it is seen today (Avdeiko et al., 2007). Such an accretion event is interpreted to be the reason for the cessation of volcanism in the Sredinny Range. Due to arc accretion at the eastern side of Kamchatka subduction jumped to its currently active position beneath the EVF and CKD. A relict of the dehydrating slab beneath the SR is interpreted to be responsible for the active volcanic activity in the westernmost volcanic chain in Kamchatka (Avdeiko et al., 2006).

Due to the southeastward motion of the Kurile-Kamchatka arc the northern part of the Kamchatka peninsula interacted with the Aleutian subduction zone and is affected since the late Miocene by the strike slip motion along the Komandorsky fault system that is kinematically connected with the Aleutian subduction zone (Fig. 1). The strike slip motion along this fault system has led to a rupture of the subducting Pacific plate at the Aleutian-Kamchatka junction (AKJ) and likely to a slab breakoff beneath northern Kamchatka between 5 and 10 Ma ago (Levin et al., 2002). As a consequence of the slab loss, volcanism ceased in northern Kamchatka and hot mantle material is interpreted to flow arc parallel southward beneath central Kamchatka (Peyton et al., 2001; Portnyagin et al., 2005). Furthermore, the slab loss has led to a decrease in the subduction angle north of the Kluchevskoy group volcanoes at the northernmost tip of the Pacific plate beneath the AKJ and likely to melting of the slab edge reflected in the geochemistry of volcanic rocks from Shiveluch volcano in northern Kamchatka (Manea and Manea 2007; Portnyagin et al., 2007). This complex tectonic setting is further influenced by the beginning subduction of the Hawaii-Emperor chain just south of the AKJ. The subduction of these remnant oceanic islands is interpreted to have a major influence on the thermal and possibly chemical structure of the northern Kamchatkan subduction zone (Manea and Manea 2007).

A remarkable, yet kinematically unresolved tectonic feature is the extension in the Central Kamchatkan Depression (CKD). The CKD opens from the South of Kamchatka and represents an active basin with westward dipping normal faults bordering its eastern side and a poorly constrained normal fault system at the western border (Kozhurin et al., 2006). Extension in the CKD began in the Upper Pliocene and is still ongoing having led to an accumulation of up to 2500m of sediments in the deepest part of the CKD (Khain 1994; Kozhurin et al., 2006). Furthermore, the CKD hosts several of the most active volcanoes on Earth, such as Kluchevskoy, Tolbachik and Shiveluch. It is remarkable that the chemistry of these CKD volcanoes is clearly distinct from that in the EVF and the SR (cf. Churikova et al., 2001; Dorendorf et al., 2000), The volcanic activity in the CKD is restricted to the northern part of the basin and only occurs where volcanism in the EVF ceases towards the North (Fig. 1).

General model assumptions

The aim of our thermodynamic-geochemical model is to predict dehydration reactions in the downgoing slab beneath Kamchatka in order to calculate the expected B concentrations and B isotopic compositions resulting from dehydration and fluid-rock interaction within the complex thermal pattern in the subducted rock pile (c.f., Konrad-Schmolke and Halama 2014). Assuming a simplified vertical migration of the liberated fluids to the source regions of the arc volcanoes, calculated positions of the dehydration reactions as well as the modeled B concentrations and B isotopic compositions of the fluids are compared with the occurrence of volcanic centers and their B geochemical characteristics. This comparison is used as an independent validation of the numerically determined dehydration pattern in the downgoing slab and wedge mantle.

In our combined thermodynamic-geochemical models, three thermal subduction zone patterns of the Northern, Central and Southern Kamchatka subduction zone (Manea and Manea, 2007) derived from finite element thermomechanical modeling (Fig. 1) are used as pressure-temperature input for a Gibbs energy minimization algorithm that simulates the passing of a vertical rock column within the subducted slab through the steady state thermal pattern (cf. Connolly, 2005; Konrad-Schmolke and Halama, 2014).

General model approach

The numerical model that we use is a combination of thermomechanical, thermodynamic and mass balanced trace element calculations. Modeling consists of the following four steps: (1) Thermal patterns of the three profiles along the Kamchatkan subduction zone are modeled, utilizing a finite element thermomechanical code, and discretized (Manea and Manea, 2007), (2) the discretized pressure-temperature-distance relations derived from the thermomechanical models are used as input for a Gibbs energy minimization algorithm that simulates the passing of a vertical rock column within the subducted slab (Connolly 2005) through the thermal input pattern. Based on the modeled pressure-temperature relations, phase relations are calculated at every discretized increment with a resolution of 250 x 250m. Water liberated by dehydration reactions is transported vertically upward equilibrating at every calculated increment within the column and thus reflecting a high ratio of fluid/slab migration velocity. (3) The modeled phase relations at every calculated increment are used for a coefficient-based mass-balanced boron distribution among the stable solid and liquid phases. (4) A temperature-dependent fluid-solid boron isotope fractionation based on experimentally determined functions (Wunder et al., 2005) is calculated to determine the amounts of ^{10}B and ^{11}B in solids and fluid. Boron incorporated into the fluid phase is assumed to migrate upward into the next calculated increment and re-distributed. Elements retained in the solids are transported within the slab and form the initial bulk rock composition in the next rock column. Therefore the model simulates fluid release, fluid migration, boron transport and boron isotope fractionation in a subducted slab passing through a steady state thermal pattern.

Thermomechanical model

The steady-state thermomechanical models of Manea and Manea (2007) consist of five thermo-stratigraphic units: the upper and lower continental crust, the oceanic lithosphere and sediments, and the mantle wedge. The boundary conditions employed in these numeric models are as following: the upper and lower boundaries correspond to 0°C and 1450°C respectively, the landward boundary is defined by a 22.5°C/km thermal gradient for the continental crust, and 10°C/km for the lithospheric mantle, and the oceanic boundary is age dependent corresponding to an oceanic geotherm calculated using GDH1 model of Stein and Stein (1992). Depth, thickness and geometry of different layers used in the 2D steady-state thermomechanical models of Manea and Manea (2007) are well constrained by seismological data. Also, the oceanic boundary conditions, that strongly control the slab thermal structure, are in good agreement with the age of the incoming Pacific plate.

Thermodynamic model

The thermodynamic model calculates modes and compositions of stable phases depending on the pressure and temperature given by the thermomechanical model and the composition of the different layers in the subducted slab. The modeled subducted slab consists of a mantle wedge layer (10 km (primitive upper mantle (PUM) of Workman and Hart 2005), a sediment pile (0.65 km (N Pacific sediment, Plank and Langmuir 1998)), igneous basaltic crust (6.5 km (N-MORB, Workman and Hart 2005)) and a variably hydrated slab mantle (18.5 km, depleted MORB mantle (DMM), Workman and Hart 2005)). Phase relations for each rock type are calculated at every increment utilizing the Gibbs energy minimization algorithm *vertex* (Connolly 2005). Thermodynamic calculations start at the bottom of the initial input column representing the initial composition of the subducted slab. Modes and compositions of the stable phases are calculated and water liberated by the modeled dehydration reactions is assumed to be transported vertically upward. Water bound in hydrous minerals is transferred slab-parallel into the corresponding increment in the next column.

Geochemical model

The modeled phase relations at every calculated increment are used for a partition coefficient-based mass-balanced boron distribution (Brenan et al., 1998) and a temperature-dependent fluid-solid boron isotope fractionation (Wunder et al., 2005).

Based on bulk distribution coefficients calculated at every increment the concentration of boron in the fluid and solids is calculated. Boron concentrated in the fluid phase is assumed to migrate vertically upward and is transferred into the next increment. Boron incorporated into solid phases is transferred slab-parallel into the corresponding increment in the next column.

Boron isotope compositions in fluid and solids are calculated at every increment based on the temperature-dependent fractionation function published in Wunder et al., (2005) and the thermal input pattern. ^{10}B and ^{11}B is distributed among the stable phases according to the calculated $\Delta^{11}B^{fluid/solid}$. Chemical and isotopic equilibration among the stable phases is assumed at every calculated increment. The isotopic evolution within the modeled system is therefore controlled by the B concentrations and the isotopic composition of B in the coexisting solid phases and the migrating fluid equilibrating with the surrounding rock. Thus, the model simulates fluid release, fluid migration, fluid-rock interaction and boron transport in a subducted slab and the overlying mantle wedge, taking into account the compositional changes of the dehydration fluid with increasing slab depth.

A comparison of modeled and observed boron concentrations and isotopic patterns is then used to evaluate the initial hydration of the slab and the dehydration behavior of wedge mantle and slab during subduction. The model presented in this work highlights the potential of combined thermodynamic-geochemical modeling and the instructive comparison with across-arc B trends.

In order to simulate water release from the slab and wedge mantle all lithologies of the incoming plate are assumed to be hydrated to different amounts. As detailed data of the hydration state of the AOC and the slab mantle offshore Kamchatka are lacking, our model constraints display simplified assumptions. The incoming sediments and the AOC are assumed to contain 7 wt% water in the sediments and 4 wt% water in the AOC (cf. Staudigel et al., 1998).

A more critical and yet unresolved question is the amount of water in the subducted slab mantle. Here we assume, in different model runs, a variable thickness (1 to 18.5 km) of hydrated oceanic mantle lithosphere that contains between 0.5 and 6 wt% water. The model runs with 2.5 wt% water in a 15 km thick hydrated slab mantle section are taken as a representative example throughout this paper, but the results of all models are evaluated and discussed. We additionally varied the most critical input parameters, such as the B concentrations and B isotopic compositions in the different layers and discuss the model sensitivity and reliability. A detailed description of the model approach and the input parameters used for the modelling is given in the electronic supplementary material.

Tracing dehydration in subduction zones using boron

The incoming oceanic lithosphere is undergoing continuous dehydration by pore compaction and dehydration reactions as it enters the subduction zone. Pore water expulsion occurs within the first 10 km depth and can be detected directly by sampling seeps and mud volcanoes in the accretionary wedges of forearcs (e.g., Mottl et al., 2004; Deyhle and Kopf 2002). In contrast, water released by metamorphic reactions occurring in the deeper parts of the subduction zone is more difficult to quantify. Commonly, continuous dehydration of the downgoing slab is deduced from across-arc trace element variations in arc volcanic rocks, in particular the concentrations, element ratios and isotopic compositions of fluid mobile elements (FMEs).

Most of these elements are abundant in the sediments and/or in the altered oceanic crust (AOC), which makes them useful tracers for the dehydration of these lithologies (e.g. Ryan et al., 1995; Elliott, 2003). However, slab mantle dehydration is most difficult to detect in arc volcanic rocks by geochemical means because ultramafic rocks are typically poor in many fluid-mobile trace elements. Arsenic, antimony, chlorine and boron (B) are among the few elements characteristic for serpentinites (Scambelluri et al., 2001; Savov et al., 2007; Spivack and Edmond 1987; Kodolàny et al., 2012) and geochemical trends of these elements as well as the isotopic composition of boron in arc lavas were interpreted to reflect serpentinite dehydration (e.g., Tonarini et al., 2011). However, geochemical models alone cannot discriminate between dehydration of serpentinites from supra-subduction zone (SSZ) mantle wedge and serpentinites from the subducted oceanic mantle. In order to make this important distinction, we use B and its isotopic composition as tracers for fluid flux and fluid-rock interaction during slab dehydration and fluid migration in a combined thermodynamic-geochemical model and compare the results to real data from the Kamchatka subduction zone.

Several unique properties of B make it particularly useful regarding the investigation of dehydration and fluid flow in subduction zones:

- B is highly fluid-mobile (Brenan et al., 1998) and its isotopic composition is influenced by temperature-dependent equilibrium fractionation between solid and fluid phases with a preferred incorporation of ^{11}B in the fluid phase (Wunder et al., 2005).

- B can be incorporated into the crystal structure of serpentine (e.g., Pabst et al., 2011) resulting in high B concentrations (up to 100 μg/g) in serpentinites (Boschi et al., 2008; Vils et al., 2008), so that dehydration of hydrated mantle rocks produces B-rich fluids that potentially create characteristic B signals in arc volcanic rocks.
- B concentrations in dry mantle rocks are extremely low (<1 μg/g), excluding significant modification of the slab signal during ascent across the mantle wedge (e.g., Ryan and Langmuir 1993).

Consequently, arc lavas are generally rich in B and have a high $\delta^{11}B$, consistent with the influence of a B-rich, high-$\delta^{11}B$ fluid derived from the subducted slab (Scambelluri and Tonarini, 2012). Across-arc trends with decreasing boron concentration and isotopically lighter compositions with increasing slab-surface depths are observed in many subduction zones (Ishikawa and Nakamura, 1994; Ishikawa and Tera, 1997; Ishikawa et al., 2001; Rosner et al., 2003). This feature is interpreted to directly reflect increasing degrees of slab dehydration and decreasing slab-to-arc element transfer (Morris et al., 1990; Moran et al., 1992; Bebout et al., 1999; Marschall et al., 2007). Several subduction zones, such as Kamchatka, show unusually high $\delta^{11}B$ and B/Nb values or characteristic reversals in their trends (Tonarini et al., 2011; Ishikawa et al., 2001; Moriguti et al., 2004), a feature that remains unexplained so far.

Chemical composition of the Kamchatkan lavas

Geochemical trends among the three different volcanic chains in Kamchatka generally fall into two groups. Proxies indicative for magmatic source components, such as high field strength element (HFSE) ratios and Nd-Hf isotopic compositions, generally show only minor variations (Dorendorf et al., 2000; Münker et al., 2004). In contrast, geochemical tracers of fluid enrichment and fluid-rock interaction, such as large ion lithophile elements (LILE), B, Li and the volatiles S, Cl and F show positive anomalies in the CKD lavas, namely in those of the Kluchevskoy group (Fig. 2).

The $\delta^{11}B$, $\delta^{18}O$ and Sr-Pb isotopic compositions clearly indicate the addition of large amounts of slab-derived fluids to the sources of the CKD lavas (e.g., Dorendorf et al., 2000; Ishikawa et al., 2001; Churikova et al., 2001, 2007). Especially boron and boron isotopic compositions of the Kamchatkan arc lavas show a characteristic pattern. In addition to the typical trend of decreasing $\delta^{11}B$ and B/Nb with increasing slab depth visible in the EVF, both parameters show a unique increase in the second volcanic chain (CKD) in Kamchatka (Fig. 1). The origin of the unusually high B/Nb and $\delta^{11}B$ in the CKD has been attributed to large influxes of slab-derived fluid (Ishikawa et al., 2001), hence making it a prime suspect for reflecting serpentinite dehydration.

Furthermore, U-series disequilibria (Dosseto and Turner 2014) indicate that the CKD lavas also show unusually fast ascent rates in the order of 20 m/a. Hence, it is widely accepted that the Kamchatkan arc volcanic rocks, especially those from the CKD, evolved in a fluid-rich subduction zone regime and fluid-triggered mantle melting is the dominant magma forming process (e.g., Churikova et al., 2007), although the source of the fluids involved in the melting processes has not been clarified so far.

Model results

Important differences in the structural position of the three thermal profiles exist. The northernmost profile cuts across the EVF chain and the CKD where the Kluchevskoy group volcanoes are located. The central profile also includes both the EVF and the CKD, but volcanic activity in the CKD is absent in this section. The third profile is located at the southernmost tip of Kamchatka, just north of the northernmost Kurile islands where the CKD is absent and the EVF displays the only active volcanic chain on the Kamchatka peninsula. The three sections show clear thermal differences between the two northern profiles and the southern profile, the latter being significantly cooler than the former two. This difference is interpreted to be due to the thermal plate rejuvenation in the northern profiles caused by the interaction of the Pacific plate with the Hawaii-Emperor plume (Manea and Manea 2007).

Simulated slab dehydration

A detailed inspection of the thermodynamic dehydration models assuming 2.5wt% water in the uppermost 15km if the slab mantle reveals that all three models yield similar patterns with respect to the dehydration of the slab crust and the overlying mantle wedge, but differ significantly in slab mantle dehydration (Fig. 3).

Forearc dehydration

In the forearc from 60 – 100 km slab surface depth, brucite, antigorite and to a lesser extent chlorite breakdown in the mantle wedge are the major water releasing reactions in all models. Amphibole, although stable in the wedge mantle, does not significantly contribute to the water budget in any of the three profiles. The modeled crustal dehydration is controlled predominantly by chlorite breakdown and is increasing to the highest values in the forearc of all models.

Sub-arc dehydration (EVF and CKD)

In the sub-arc region underneath the EVF, water is delivered by continuous chlorite dehydration from the crust and, in case of the northern profile, by the chlorite-out reaction in the wedge mantle that causes a characteristic peak in this model at ~130 km slab surface depth. The lawsonite-out reaction starts at about 100km depth and is dominating the water release from the subducted slab crust up to ~250 km slab surface depth. The overall dehydration pattern resulting from these reactions is characterized by a significant decrease between 90 and 110 km depth followed by a significant increase with a maximum at about 120 km slab depth and a more constant dehydration down to 250 km slab surface depth (Fig. 3). The drastic increase in the water release beneath the EVF is caused by increasing chlorite dehydration in the crust and the SSZ mantle.

The most important result of our models, however, concerns the spike-like water release from the slab mantle by the antigorite breakdown reactions in the northern and central profile (arrows in the upper panels in Fig. 3). The antigorite-out reaction starts at the bottom of the hydrated slab mantle part (Fig. 3, lower panel). Here, the liberated water migrates upward until it reaches a water-undersaturated part of the slab mantle, where it is resorbed and dragged down within the plate. This process is repeated until the thermal stability limit of antigorite in the slab mantle is reached. Here, the accumulated water is released, which causes very high fluid fluxes and a narrow spike-like peak in the water release in the northern profile at about 175 km depth. In contrast, water liberated at the topmost part of the hydrated slab mantle directly migrates upward into the slab crust, which can be seen in the central profile, where slab mantle dehydration causes a more gradual water liberation between 175 and 200 km slab depth. Nevertheless, in both cases large amounts of water are liberated by antigorite breakdown causing a massive fluid flux into the overlying slab crust and wedge mantle. The position of this reaction coincides well with the location of the second volcanic chain in the CKD in the northern profile and with the position of the CKD basin in the southern profile. Beyond the CKD, minor water release continues by lawsonite breakdown in the crustal part of the slab.

In contrast to the northern and central profiles, slab mantle dehydration as observed in the other two models is completely absent in the southern profile. Due to the lower slab temperatures water liberation due to antigorite breakdown is lacking and the entire water stored in the hydrous slab mantle is subducted beyond sub-arc depth.

Boron modelling

Figure 4 shows the result of a mass balanced boron distribution among the modeled stable phases in Fig. 3, together with a temperature-dependent fluid/solid boron isotope fractionation. These models provide information about the B geochemical characteristics of the slab-derived fluid as it enters the melting region underneath the arc. Comparing the modeled values with observed data from arc lavas serves as an independent test for the quantitative validity of the thermodynamic model results.

The uppermost panel in Fig. 4 shows the boron concentration (μg/g) in the liberated fluid (green line) as well as the modeled boron flux ($kg/m^2/s$) into the mantle wedge (red line). The drastic increase in boron release beneath the CKD is predominantly controlled by the fluid amount rather than by the concentration of B in the fluid. In the southern profile this B peak is missing as there is no slab mantle dehydration occurring.

All models can reproduce the characteristic decreasing B concentrations (reflected in the decreasing B/Nb ratios, where Nb represents a fluid-immobile reference element) in the lavas of the EVF and the northern profile model successfully reproduces the observed high values in the CKD volcanoes (cf. Figs. 1 and 4).

The observed $\delta^{11}B$ values in Kamchatka (second and lowermost panel in Fig. 4) show a continuous linear decrease in the EVF as well as a distinct increase in the CKD volcanoes. Our models can reproduce both features. In all models the dehydration of each lithology in the layered slab is associated with continuous dehydration-induced $\delta^{11}B$ depletion in the residual rocks leading to a decreasing $\delta^{11}B$ trend in the released fluids. First, dehydration of sediments and SSZ wedge serpentinites releases extremely heavy boron into the fore-arc region, a feature that is observed in many forearcs. Subsequently, initial dehydration of the oceanic crust releases high-$\delta^{11}B$ fluids initiating a second trend of decreasing $\delta^{11}B$ that is recorded in the EVF and in several other arcs globally. Finally, the high-B fluid released by antigorite breakdown in the slab mantle of the northern and central profiles directly transfers a high- $\delta^{11}B$ signature towards the surface due to the high water flux and the finite capability of the crust to incorporate B. It is notable that continuing dehydration of slab crust alone is not able to deliver any significant amounts of water or boron at depths greater than 150 km. This is due to the fact that phengite, the phase with the highest B concentration in the oceanic crust, remains stable to beyond arc depths. Moreover, any released crustal fluids are expected to carry a negative $\delta^{11}B$ value due the loss of isotopically heavy B during early stages of subduction, inconsistent with the observed positive $\delta^{11}B$ in the CKD volcanic rocks. Both, the modeled drastic water release from the slab together with the anomalously high [B] and $\delta^{11}B$ values associated with slab mantle dehydration strengthen the hypothesis that the CKD volcanic activity is induced by devolatilisation of the subducted oceanic mantle.

Water subducted beyond arc

Figure 5 shows a summary of the modeled water contents of the slab and the water subducted beyond arc. The latter is displayed in vertical sections through the slab at maximum slab depth in the three models. In all models dehydration reactions ceased at the maximum model depth and the only stable hydrous phases in all slabs are phengite and phase A in the oceanic crust/sediments and mantle, respectively.

Three features are important to mention regarding the water content of the slab. First, in none of the models the SSZ mantle is able to bring water beyond the first volcanic chain, so ruling out its role in deep water recycling. Second, the sedimentary layer is capable of bringing 0.9 wt% water to depth greater than 250 km whereas the water content in the MORB layer is with 0.03 wt% negligible after lawsonite dehydration. In both lithologies phengite is the only hydrous mineral that is stable at depths greater than 250km and the amount of water subducted to these depths is proportional to the potassium content of the oceanic crust and the sedimentary pile (cf. Hacker 2008). Despite its limited thickness of less than 1 km, however, the 0.9 wt% water in the sedimentary layer make up 75% of the deeply subducted water in the oceanic crust (excluding the slab mantle). Third, the amount of water subducted in the slab mantle part beyond the volcanic arc is controlled by the overlap of the stability fields of antigorite and phase A as well as by the amount of phase A stable in the slab mantle.

The bell shaped curves in the right-hand diagrams show the maximum capacity of Phase A to bring water beyond the arc in the northern and central profiles. This value is already reached by the models assuming 2.5wt% water in a 15 km thick mantle part. Additional water from the serpentinized slab mantle is released into the overlying mantle wedge. In contrast, in the colder southern profile dehydration reactions are lacking as all water in the slab mantle can be transferred into Phase A. A summary of the calculated beyond-arc water fluxes corresponding to the models in Fig.5 is given in Table 1.

It is evident that only in case of the northern profile, where a second volcanic chain is indicating slab mantle dehydration, constraints can be made on the beyond arc water subduction. Fluid liberation from the slab mantle is here indicating that the water saturation in the deeper slab mantle (controlled by Phase A) has been overcome. In the northern profile the water saturation in the beyond arc slab is controlled by the bell-shaped profile vertically across the stability field of Phase A (Fig. 4), this curve can be used to calculate the minimum amount of water in the subducted slab necessary to saturate the slab beyond arc.

The relation between the beyond-arc water flux in the northern profile and the depth of initial hydration of the subducted slab mantle is shown in Fig. 6. The sigmoidal curve is reflecting the bell-shaped water saturation profile in Fig. 5. The bold numbers on that curve show the minimum initial water content of the slab mantle that is necessary to yield a fully hydrated beyond-arc slab mantle (controlled by the amount of Phase A). ~~A~~t this minimum water content, no slab mantle dehydration would occur and no second volcanic chain could develop, as the values represent the minimum amount of water necessary to fully hydrate Phase A. In the case of the northern and central profiles, however, slab mantle dehydration does occur and the $\delta^{11}B$ signal in the arc lavas can be used to determine the actual extent of slab mantle dehydration as the $\delta^{11}B$ signal is a function of the excess water released from the slab. The slab mantle water content necessary to reproduce the observed $\delta^{11}B$ patterns in the CKD volcanic lavas is indicated by the numbers in italics on the grey curve. Our results show that the beyond-arc arc water flux in Kamchatka is between ~1.1 x 10^3 and ~7.4 x 10^3 $TgMa^{-1}km^{-1}$, equal to between 0.75 and 5.2 x 10^6 $TgMa^{-1}$ over the entire 700 km subduction zone length (Fig. 6). The upper boundary of this value is constrained by the amount of water that can be stored in stable phase A. The lower boundary of 0.75 x 10^6 $TgMa^{-1}$ is given by the constraint to reproduce the observed $\delta^{11}B$ pattern, which is not possible at hydration depths smaller than 2.5 km.

Discussion

Critical parameters of our model

Due to the large number and complexity of the input parameters of our model a detailed examination of the critical parameters is necessary. Generally, as argued afore, we interpret that the complex across-arc B pattern observed in Kamchatka can excellently explained by a succession of slab crust and subsequent slab mantle dehydration. Consequently it has to be questioned inasmuch a comparison of modeled and observed B patterns can be used to quantify the hydration state of the subducted slab mantle and the absolute amount of water subducted beyond arc in Kamchatka.

Critical parameters for the water cycling in subduction zones are the hydration intensity and the hydration depth of the subducting slab mantle (Rüpke et al., 2006; Hacker 2008; van Keken et al., 2011; this study). Both of these input parameters influence the boron signal of the CKD arc volcanic rocks (Fig. 6). Distinct model runs, which differ in initial water content and hydration depth of the slab mantle, can therefore reproduce the complex pattern observed in the CKD volcanic rocks.

Other critical parameters of our model and the effect of their variation on the results are shown in Fig. 7. The parameters with the largest influence on the modeled $\delta^{11}B$ values are the initial B concentration and $\delta^{11}B$ of the MORB and the slab mantle as well as the B fluid-lawsonite distribution coefficient. In contrast, it is evident in Fig. 7 that neither the B concentration and $\delta^{11}B$ in the SSZ mantle nor in the sediments influence the B pattern in the CKD lavas significantly. Interestingly, the concentration of B in the MORB layer has the largest effect on the $\delta^{11}B$ in the CKD lavas, whereas initial $\delta^{11}B$ in MORB is influencing the subarc (EVF) $\delta^{11}B$ pattern. This result is reflecting the filter effect of the MORB layer. A B-poor MORB layer will have little effect on the B concentration and $\delta^{11}B$ of fluids derived from the slab mantle. Thus, in case of a B-poor oceanic crust the $\delta^{11}B$ signal from the slab mantle is directly transferred to the slab surface and the magma source region. A scenario, however, with a B-rich slab mantle and a B-poor slab crust, which could equally reproduce the observed $\delta^{11}B$ pattern, is quite unlikely as B is transferred to both lithologies by the ocean water, more of which is certainly interacting with the crust than the mantle. It has to be noted, however, that the filter effect of the MORB crust is essential for determining the absolute $\delta^{11}B$ values in the CKD volcanoes.

In general the $\delta^{11}B$ pattern in the EVF volcanoes can be used to constrain several of the critical parameters used for the interpretation of the B signal in the CKD lavas (Fig. 6). Variations in the lawsonite-fluid distribution coefficient as well as the initial $\delta^{11}B$ in the MORB crust yield distinct $\delta^{11}B$ patterns in the EVF lavas, which can be used to constrain these values.

However, since the across-arc geochemical variations alone do not yield unambiguous information on the hydration state parameters, but only on their relations (Fig. 6) seismic constraints on the hydration depth of the slab mantle prior to subduction, together with thermodynamic models as presented in this work, are required to fully quantify the water budget in subduction zones. To our knowledge, there are no data available that constrain the degree of hydration of the oceanic mantle east of the Kamchatka trench, but normal faults, fault escarpments and fracture zones have been identified by geophysical methods in the upper mantle of the adjacent Japan and Kurile trenches (Garth and Rietbrock 2011; Kobayashi et al., 1998). All of these features facilitate hydration of the incoming oceanic mantle. Whether slab mantle dehydration is significant elsewhere has to be evaluated considering thermal and thermodynamic constraints for each subduction zone individually.

Distinction between fluid source rocks

All subducted hydrated lithologies potentially contribute to the water budget in the subduction zone, but it is only the hydrated slab mantle that is able to transfer significant amounts of water into the deeper mantle in antigorite (e.g., Ulmer and Trommsdorff 1995) and subsequently DHMS (Phase A). Hence, detection of slab mantle dehydration serves as an indicator for possible deep water recycling and according to our models the volcanic activity in the CKD, occurring up to 200km above the subducted slab, is providing indirect evidence for slab mantle hydration in Kamchatka.

It is evident that both the EVF and the CKD are reflecting a strong contribution of slab-derived fluids to the zone of magma generation (e.g., Dorendorf et al., 2000; Churikova et al., 2001; 2007; Portnyagin et al., 2005). Based on trace element modeling, the fluid contribution to the melts seems to be highest (up to 2.1%) in the CKD volcanoes (Churikova et al., 2001). This interpretation is supported by the data shown in Fig. 2: The Ba/Nb as well as the Ba/Th ratios show similar trends, i.e. a slight decrease with increasing slab depth in the EVF followed by a clear increase in the CKD volcanic rocks, indicating an increasing contribution of slab-derived aqueous fluids on the melt sources of the CKD volcanoes. In contrast the Th/Nb ratios, possibly indicative for hydrous melts derived from the downgoing slab (e.g., Perce et al., 2005) are largely constant in both volcanic chains. Hence, the majority of the geochemical data are in general agreement with a strong fluid contribution to the arc volcanic lavas in Kamchatka, but the source of these fluids remains to be clearly characterised.

Churikova et al. (2007) could show that the fluid sources for the EVF and CKD volcanoes are chemically distinct, the latter being characterized by elevated $^{87}Sr/^{86}Sr$ ratios and high $\delta^{18}O$, whereas the EVF fluids are characterized by high LILE and LREE contents, but also high concentrations in F and chalcophile elements. Based on their observations they distinguish between serpentine + amphibole and lawsonite + phengite for the dehydrating mineral assemblages beneath the EVF and the CKD, respectively.

In contrast, our thermodynamic models suggest a strong contribution of chlorite dehydration in both, the SSZ mantle as well as the MORB crust, to the fluids causing the EVF volcanism (Fig. 3). The high B content of the EVF lavas comes from the fluid-rock interaction and the resulting B enrichment in fluid during the fluid percolation through the oceanic crust and the sediment layer (Fig. 4). The $\delta^{11}B$ patterns in all three modeled profiles are also in agreement with that interpretation. Regarding the second fluid source, beneath the CKD volcanoes, our northern and central profiles clearly show that dehydration of sediments, hydrated crust and SSZ wedge mantle, cannot deliver enough water to explain the high B/Nb or the high $\delta^{11}B$ values in the CKD lavas (Fig. 4). Phengitic white mica, known to be a significant carrier of B in sedimentary and igneous lithologies in subduction zones (Bebout et al., 2007; Konrad-Schmolke et al., 2011a; Bebout et al., 2013; Halama et al., 2014), remains stable in the crustal parts of the slab and does therefore neither contribute to fluid release thereof nor to release of other FMEs preferentially incorporated into phengite. This is consistent with experimental constraints on the stability of phengite to depths exceeding 360 km (Domanik et al., 1996) and field-based evidence for the retention of FME in phengite-bearing HP rocks (Bebout et al., 2007; Bebout et al., 2013). Due to the comparatively small volume and the strongly negative $\delta^{11}B$ values, neither the amount nor the isotopic composition of B (Fig. 4) in the sediments beneath the CKD can account for the high B flux and the high $\delta^{11}B$ in the CKD lavas.

Several studies have shown that the SSZ mantle wedge can be dragged down to sub-arc depths and contribute significantly to the melt production and trace element transfer in subduction zones (Hattori and Guillot 2003; Savov et al., 2007; Tonarini et al., 2011). In cases where hydrated SSZ wedge material is dragged down to below the volcanic front, a heavy B isotope signature may be transferred into the arc front volcanic rocks, as proposed for the Izu arc (Straub and Layne 2002) and the South Sandwich Island arc (Tonarini et al., 2011). All of our three models predict the release of isotopically heavy B into forearc and subarc underneath the EVF due to dehydration of sediments and SSZ wedge serpentinite, which is consistent with observations from serpentinite seamounts (Benton et al., 2001) and highlights the important role of wedge mantle dehydration for volcanism in other arcs (Tonarini et al., 2011). However, the thermal stability of chlorite in the Kamchatka mantle wedge limits the depth to which this reservoir is able to deliver water and trace elements into the magma source regions to about 130 km depth-to-slab. Hence, the thermal structures of the chosen profiles, which are constrained by independent observations (Manea and Manea 2007), do not suggest that SSZ mantle wedge is dehydrating underneath the CKD. To explain volcanic activity in this second volcanic chain and elevated $\delta^{11}B$ and high B contents in the CKD arc lavas, our models provide an alternative mechanism: the dehydration of slab serpentinite. B-rich fluids derived from slab mantle dehydration beneath the CKD volcanoes transport a high $\delta^{11}B$ signal from the slab to the melt source region (Fig. 3B and C), explaining the observed across-arc variations in B/Nb and $\delta^{11}B$. Moreover, the high K/Nb, Rb/Nb, Ba/Nb, Pb/Nb and Zr/Y ratios that characterize the CKD lavas (Dorendorf et al., 2000) likely result from slab mantle fluid release as the more fluid-mobile species (K, Rb, Ba and Pb) are scavenged via fluid percolation through the sediment layer. High $\delta^{18}O$ values observed at Kluchevskoy volcano, previously attributed to dehydration of low-temperature altered oceanic crust (Dorendorf et al., 2000), can equally well be explained by slab mantle dehydration if low serpentinisation temperatures and/or serpentinisation at/near the seafloor are assumed.

Our argument of slab mantle dehydration is further supported by the observation of a double seismic zone in Kamchatka (Gorbatov et al., 1997). Such double seismic zones are commonly explained to result from dehydration reactions up to several tens of kilometers within the subducted plate (Hacker et al., 2003). In case of our models such dehydration reactions can be explained by slab mantle dehydration that starts at the base of serpentinite stability within the subducted slab (Fig. 2). Dehydration and subsequent fluid migration within the slab mantle can likely be a source for the observed seismicity in the lower zone of the double seismic zone in the Kamchatkan slab.

Slab melting

Another critical aspect is the mass balanced distribution of boron between liquid and solid phases. Slab surface temperatures in our model (650-750°C at 100-150 km slab depth) are hot enough to allow fluid-induced flux melting in the sediment layer to the rear of the EVF, as suggested for Kamchatka based on geochemical parameters (Duggen et al., 2007; Plank et al., 2009). Such fluxed melting of the sediment layer could indeed be triggered by the dehydration of the underlying AOC or the serpentinized slab mantle and the relatively high Th/Nb in some of the EVF lavas (Fig.2) might be the result of flux-melting of the subducted sediments. However, our models do not consider melts due to the lack of reliable thermodynamic data, but instead assume that the slab-derived liquid is an aqueous fluid. Experimental data suggest that fluids leaving the slab are in a supercritical state and complete miscibility between solute-rich fluid and aqueous melts might exist (Hermann et al., 2006; Mibe et al., 2011). We argue that a distinction between melt and fluid is of minor importance in our model, because the changes of B solid-liquid partition coefficients remain fairly constant over a wide temperature range

(700-1200 °C) and different liquid compositions (Kessel et al., 2005). Moreover, we assume that all B released from the slab is incorporated into the melt phase in shallower regions of the mantle wedge where the B compositional and isotopic information is transferred into the source melts of the arc lavas. Melting of the igneous crust of the slab under water-saturated conditions, producing eclogite-derived melts, has also been proposed for the origin of the peculiar geochemical characteristics of the CKD volcanoes (Yogodzinski et al., 2001). However, these melts are highly reactive with peridotite and efficient transport through the mantle wedge is unlikely (Portnyagin and Manea 2008). Instead, compositional trends within the CKD may be related to a decrease of magma generation temperature and length of mantle melting columns toward the slab edge (Portnyagin and Manea 2008).

Along-arc versus across-arc variations

The geochemical data used here for comparative purposes were originally plotted versus increasing slab depth and interpreted in terms of across-arc variations (Ishikawa et al., 2001). However, the position of the volcanoes sampled forms a line that is oblique to the subduction direction, with depth-to-slab increasing from south to north. Hence, the comparison of the modeled geochemical variations, which are based on a thermal model aligned parallel with the convergence velocity, and the observed geochemical data is simplifying the geodynamic situation. Noting that other "across-arc" trends also include volcanoes covering along-arc variation of several 10s to 100s km, e.g. about 60 km in Japan (Ishikawa and Nakamura 1994), about 300 km across the Andes (Rosner et al., 2003) and nearly 1000 km at the Kurile trench (Ishikawa and Tera 1997), we emphasize that deviations from a perfectly aligned across-arc profile are unavoidable for most natural data sets and do not challenge the principal findings of our model. It is notable that some of the geochemical parameters that support our interpretation, such as the data of Churikova et al., 2001, are indeed sampled along an across-arc profile largely perpendicular to the volcanic chains. Nevertheless, despite the wealth of data available for the Kamchatkan subduction zone today none of the published geochemical datasets allows an unambiguous interpretation of the across-arc variations in Kamchatka. We further emphasize that there is an along-arc variation in the slab temperature pattern (Fig. 1), which is why we decided to use three different profiles for our thermodynamic models in order to account for this along-arc temperature variation.

Slab-to-arc transport of geochemical signals

The idea that chemical processes in the subducting slab are reflected in the chemistry of arc volcanic rocks is an important, but strongly debated assumption (e.g., Pearce and Peate 1995; Marschall and Schumacher 2012). Based on the coincidence between modeled and observed across-arc geochemical signatures and the correlation between thermodynamically predicted positions of water release and the occurrences of volcanic centers in Kamchatka, we assume that there is a clear, fluid-mediated link between arc lava geochemistry and slab processes for the Kamchatka subduction zone. As our models are simplified with respect to a strictly vertical fluid migration it was a clear overinterpretation to suggest a strictly vertical melt transport in the Kamchatkan subduction zone. A major implication of our results is, however, that the geochemical signature visible in the arc volcanic rock in Kamchatka is generated in the subducting slab already (by fluid-rock interaction) and transferred (sub-vertically) to the melt sources by a fluid phase. These findings are in agreement with previously postulated direct delivery of fluids to the melting region and the preservation of trace element characteristics from fluid source lithologies (Hebert et al., 2009). Further, the rapid magma ascent underneath the Kamchatka volcanoes indicated by U-series disequilibria (Dosseto and Turner 2014), is also pointing towards a direct slab-to-arc transfer. Such a direct, almost vertical slab-to-arc transfer of geochemical signatures questions models that invoke other means of slab-to-arc transport (Gerya and Yuen 2003; Behn et al., 2011; Marschall and Schumacher 2012), at least in fluid-dominated subduction systems like Kamchatka.

Comparison with other previous estimates of beyond arc water fluxes

A comparison of our model data with those of Hacker (2008) and Van Keken et al. (2011) – the only two estimates for beyond arc water flux in Kamchatka – shows that although they are lower in the initial water content of the oceanic mantle, their absolute values of water subducted beyond arc are higher than our estimates (Fig. 7). This difference is likely reflecting different model approaches. Whereas both Hacker (2008) and Van Keken et al. (2011) utilize one dimensional thermodynamic models we consider internal water redistribution within the different lithologies, which leads to an inhomogeneous water distribution in the slab mantle layer and different beyond arc water fluxes. This effect seems to play a major role regarding the water budget in subduction zones. Fig. 7 also shows that the values yielded from our models are at the lower end of the range of previously published global average beyond arc water fluxes.

Concluding remarks

In the last decade the deep water recycling in subduction zones came into focus of several scientific investigations (Rüpke et al., 2004; Hacker 2008; Parai and Mukhopadhyay 2012; Van Keken et al., 2011). All studies of subduction zone water cycling, including the one presented here, have concluded that hydrated oceanic mantle is the most effective lithology regarding deep water recycling (Rüpke et al., 2004; Hacker 2008; Van Keken et al., 2011). Reliable quantification of the Earth's deep water cycle is therefore only possible with knowledge about the hydration state and the dehydration behavior during subduction of the subducted oceanic mantle. Regarding the hydration state of the oceanic mantle entering the subduction zones, so far only a few segments of the global subduction zones are investigated, but most of these studies show either strongly hydrated oceanic mantle or at least a deeply fractured oceanic lithosphere potentially allowing for strong hydration of the incoming oceanic plate (e.g., Ranero et al., 2003). These observations suggest that the incoming oceanic plate is hydrated to a much higher degree than previously thought.

Kamchatka is a unique example of a well-investigated subduction zone with plenty of published geophysical and geochemical data. The exceptional situation of three successive volcanic chains additionally allows studying of slab processes at different depths. Therefore we want to point out the importance of Kamchatka for further investigations of the global deep water cycle.

In this contribution we used modeled and observed data available for Kamchatka for an integrated thermodynamic-geochemical model in order to set constraints on possible deep water recycling in the oceanic mantle and its possible contribution to the global water cycle. Our results show that the beyond-arc arc water flux in Kamchatka is between ~1.1×10^3 and ~7.4×10^3 $TgMa^{-1}km^{-1}$, equal to between 0.75 and 5.2×10^6 $TgMa^{-1}$ over the entire 700 km subduction zone length. These values are significantly lower than previous estimates for the Kamchatkan subduction zone (Hacker 2008; Van Keken et al., 2011) and are at the lower end of previsouly published global beyond arc water fluxes. Nevertheless, given the lack of information about the hydration state of the oceanic mantle offshore Kamchatka, these models yield indirect evidence for significant beyond-arc water subduction.

ACKNOWLEDGMENTS. This work was supported by DFG grant KO 3450/2. We thank M. Trauth and J. Connolly for advice in programming the numerical codes. We further thank the reviewers in advance for their comments

References

Angel RJ, Frost DJ, Ross NL, Hemley R (2001) Stabilities and equations of state of dense hydrous magnesium silicates. *Phys. Earth Planet. Interiors* 127:181-196.

Avdeiko GP, Palueva AA, Khleborodova OA (2006) Geodynamic conditions of volcanism and magma formation in the Kurile-Kamchatka island-arc system. *Petrology* 14:230-246.

Avdeiko GP, Savelyev DP, Palueva AA, Popruzhenko SV (2007) Evolution of the Kurile-Kamchatkan volcanic arcs and dynamics of the Kamchatka-Aleutian junction. *Geophysical Monograph Series* 172:37-55.

Bebout GE, Bebout AE, Graham CM (2007) Cycling of B, Li, and LILE (K, Cs, Rb, Ba, Sr) into subduction zones: SIMS evidence from micas in high-P/T metasedimentary rocks. *Chem Geol* 239:284-304.

Bebout GE, Ryan JG, Leeman WP, Bebout AE (1999) Fractionation of trace elements by subduction-zone metamorphism – effect of convergent-margin thermal evolution. *Earth Planet Sci Lett* 171:63–81.

Bebout GE, Agard P, Kobayashi K, Moriguti T, Nakamura E (2013) Devolatilization history and trace element mobility in deeply subducted sedimentary rocks: Evidence from Western Alps HP/UHP suites. *Chem Geol* 342:1-20.

Benton LD, Ryan JG, Tera F (2001) Boron isotope systematics of slab fluids as inferred from a serpentine seamount, Mariana forearc. *Earth Planet Sci Lett 187:273-282.*

Boschi C, Dini A, Früh-Green GL, Kelley DS (2008) Isotopic and element exchange during serpentinization and metasomatism at the Atlantis Massif (MAR 30°N): Insights from B and Sr isotope data. *Geochim Cosmochim Acta* 72 1801-1823.

Brenan JM, Ryerson FJ, Shaw HF (1998) The role of aqueous fluids in the slab-to-mantle transfer of boron, beryllium, and lithium during subduction: Experiments and models. *Geochim Cosmochim Acta* 62:3337-3347.

Brown M. (2008) Characteristic thermal regimes of plate tectonics and their metamorphic imprint throughout Earth history: When did Earth first adopt a plate tectonics mode of behavior. *Geological Society of America Special Papers, 440:97-128.*

Churikova, T., Dorendorf, F., and Wörner, G. (2001). Sources and fluids in the mantle wedge below Kamchatka, evidence from across-arc geochemical variation. *Journal of Petrology*, *42*(8), 1567-1593.

Churikova, T., Wörner, G., Mironov, N., and Kronz, A. (2007). Volatile (S, Cl and F) and fluid mobile trace element compositions in melt inclusions: implications for variable fluid sources across the Kamchatka arc. *Contributions to Mineralogy and Petrology*, *154*(2), 217-239.

Condie KC, Kröner A (2008) When did plate tectonics begin? Evidence from the geologic record. *Geological Society of America Special Papers 440:281-294.*

Connolly JAD (2005) Computation of phase equilibria by linear programming: A tool for geodynamic modeling and its application to subduction zone decarbonation. *Earth Planet Sci Lett* 236:524-541.

Deyhle A, Kopf A (2002): Strong B enrichment and anomalous $\delta^{11}B$ in pore fluids from the Japan Trench forearc. *Marine Geology* 183:1-15.

Domanik KJ, Holloway JR (1996) The stability and composition of phengitic muscovite and associated phases from 5.5 to 11 GPa: Implications for deeply subducted sediments. *Geochim Cosmochim Acta* 21:4133-4150.

Dorendorf F, Wiechert U, Wörner G (2000) Hydrated sub-arc mantle: a source for the Kluchevskoy volcano, Kamchatka/Russia. *Earth Planet Sci Lett* 175:69-86.

Dosseto, A., and Turner, S. (2014). Reappraisal of uranium-series isotope data in Kamchatka lavas: implications for continental arc magma genesis. *Geological Society, London, Special Publications*, *385*(1), 103-116.

Duggen S. S., Portnyagin, M., Baker, J., Ulfbeck, D., Hoernle, K., Garbe-Schönberg, D., and Grassineau, N. (2007) Drastic shift in lava geochemistry in the volcanic-front to rear-arc region of the Southern Kamchatkan subduction zone: Evidence for the transition from slab surface dehydration to sediment melting. *Geochim Cosmochim Acta* **71**:452-480.

Elliott T (2003) Tracers of the slab. *Geophys Monogr Ser* 138:23-45.

Freundt, A., Grevemeyer, I., Rabbel, W., Hansteen, T. H., Hensen, C., Wehrmann, H., Frische, M. (2014) Volatile budget of the Central American subduction zone. *Int J Earth Sci* 10.1007/s00531-014-1001-1.

Frost DJ (1999) The stability of dense hydrous magnesium silicates in Earth's transition zone and lower mantle. In: Mantle Petrology: Field Observations and High Pressure Experimentation: A Tribute to Francis R. (Joe) Boyd, Eds. Y. Fei, C.M. Bertka, B.O. Mysen. Geochemical Society, Special Publication 6:283-296.

Garth T, Rietbrock A (2014) Order of magnitude increase in subducted H_2O due to hydrated normal faults within the Wadati-Benioff zone. *Geology* 10.1130/G34730.1.

Gerya TV, Yuen DA (2003) Rayleigh-Taylor instabilities from hydration and melting propel "cold plumes" at subduction zones. *Earth Planet Sci Lett* 212:47-62.

Gorbatov, A., Kostoglodov, V., Suárez, G., and Gordeev, E. (1997). Seismicity and structure of the Kamchatka subduction zone. *Journal of Geophysical Research: Solid Earth*, *102*(B8), 17883-17898.

Hacker BR (2008) H_2O subduction beyond arcs. *Geochem Geophys Geosyst* 9 (Q03001): 10.1029/2007GC001707.

Hacker BR, Peacock SM, Abers GA, Holloway SD (2003) Subduction factory 2. Are intermediate-depth earthquakes in subducting slabs linked to metamorphic dehydration reactions? *J Geophys Res* 108, B1, 2030, doi:10.1029/2001JB001129.

Halama R, Konrad-Schmolke M, Sudo M, Marschall HR, Wiedenbeck M (2014) Effects of fluid–rock interaction on $^{40}Ar/^{39}Ar$ geochronology in high-pressure rocks (Sesia-Lanzo Zone, Western Alps). *Geochim Cosmochim Acta* 126:475-494.

Hallam A (1984) Pre-Quaternary sea-level changes. *Annu Rev Earth Planet Sci* 12:205-243.

Haq BU, Hardenbol J, Vail PR (1987) Chronology of fluctuating sea levels since the Triassic. *Science* 235:1156-1167.

Haq BU, Schutter SR (2008) A chronology of Paleozoic sea-level changes. *Science* 322:64-68.

Hattori K, Guillot S (2003) Volcanic fronts form as a consequence of serpentinite dehydration in the forearc mantle wedge. *Geology* 31:525-528.

Hebert LA, Asimow P, Antoshechkina P (2009) Fluid source-based modeling of melt initiation within the subduction zone mantle wedge: Implications for geochemical trends in arc lavas. *Chem Geol* 266:297-310.

Hermann J, Spandler C, Hack A, Korsakov AV (2006) Aqueous fluids and hydrous melts in high-pressure and ultra-high pressure rocks: Implications for element transfer in subduction zones. *Lithos* 92:399-417

Ishikawa T, Nakamura E (1994) Origin of the slab component in arc lavas from across-arc variation of B and Pb isotopes. *Nature* 370, 205-208.

Ishikawa T, Tera F (1997) Source, composition and distribution of the fluid in the Kurile mantle wedge: Constraints from across-arc variations of B/Nb and B isotopes. *Earth Planet Sci Lett* 152:123-138.

Ishikawa T, Tera F, Nakazawa T (2001) Boron isotope and trace element systematics of the three volcanic zones in the Kamchatka arc. *Geochim Cosmochim Acta* 65:4523-4537.

Jacobsen SD, Van Der Lee S. (Editors) (2006) Earth's Deep Water Cycle. Geophysical Monograph Series, Volume 168. American Geophysical Union, Washington, DC.

Karato S (2011) Water distribution across the mantle transition zone and its implications for global material circulation. *Earth Planet Sci Lett* 301:413–423.

Kessel R, Schmidt MW, Ulmer P, Pettke T (2005) Trace element signature of subduction-zone fluids, melts and supercritical liquids at 120–180 km depth. Nature 437:724-727.

Khain VE (1994) Geology of the Northern Eurasia, second part: Phanerozoic fold belts and young platforms, Beiträge zur regionalen Geologie der Erde, Bd. 24, Borntraeger, Berlin, Stuttgart.

Kimura JI et al. (2009) Arc Basalt Simulator version 2, a simulation for slab dehydration and fluid-fluxed mantle melting for arc basalts: Modeling scheme and application. Geochem Geophys Geosyst 10 (Q09004): 10.1029/2008GC002217.

Kobayashi K, Nakanishi M, Tamaki K, Ogawa Y (1998) Outer slope faulting associated with the western Kuril and Japan trenches. *Geophys J Int* 134:356-372.

Kodolányi J, Pettke T, Spandler C, Kamber BS, Gméling K (2012) Geochemistry of ocean floor and fore-arc serpentinites: constraints on the ultramafic input to subdcution zones. J Petrol 53:235-270.

Konrad-Schmolke, M., and Halama, R. (2014). Combined thermodynamic–geochemical modeling in metamorphic geology: Boron as tracer of fluid–rock interaction. *Lithos*, *208*, 393-414.

Konrad-Schmolke M, Zack T, O'Brien PJ, Barth M (2011) Fluid migration above a subducted slab — Thermodynamic and trace element modelling of fluid–rock interaction in partially overprinted eclogite-facies rocks (Sesia Zone, Western Alps). *Earth Planet Sci Lett* 311:287-298.

Kozhurin, A., Acocella, V., Kyle, P. R., Lagmay, F. M., Melekestsev, I. V., Ponomareva, V., ... and Rovida, A. (2006). Trenching studies of active faults in Kamchatka, eastern Russia: Palaeoseismic, tectonic and hazard implications. *Tectonophysics*, *417*(3), 285-304.

Levin, V., Park, J., Brandon, M., Lees, J., Peyton, V., Gordeev, E., Ozerov, A., 2002: Crust and upper mantle of Kamchatka from teleseismic receiver functions. Tectonophysics 358: 233-265.

Manea VC, Manea M (2007) Thermal models beneath Kamchatka and the Pacific Plate rejuvenation from a mantle plume impact. *Geophys. Monogr. Ser.* 172:77-90.

Marschall HR, Altherr R, Rüpke L (2007) Squeezing out the slab – modelling the release of Li, Be and B during progressive high-pressure metamorphism. *Chem Geol* 239:323-335.

Marschall HR, Schumacher JC (2012) Arc magmas sourced from mélange diapirs in subduction zones. *Nat Geosci* 5:862-867.

Marty, B. (2012). The origins and concentrations of water, carbon, nitrogen and noble gases on Earth. *Earth and Planetary Science Letters*, *313*, 56-66.

Maruyama S, Okamoto K (2007) Water transportation from the subducting slab into the mantle transition zone. *Gondwana Research* 11:148-165.

Mei S, Kohlstedt DL (2000) Influence of water on plastic deformation of olivine aggregates 1. Diffusion creep regime. *J Geophys Res* 105:21457-21469.

Mibe K, Kawamoto T, Matsukage N, Fei Y, Ono S (2011) Slab melting versus slab dehydration in subduction-zone magmatism. *P Natl Acad Sci USA* 108:8177-8182.

Moran AE, Sisson VB, Leeman WP (1992) Boron depletion during progressive metamorphism: implications for subduction processes. *Earth Planet Sci Lett* 111:331–349.

Moriguti T, Shibata T, Nakamura E (2004) Lithium, boron and lead isotope and trace element systematics of Quaternary basaltic volcanic rocks in northeastern Japan: mineralogical controls on slab-derived fluid composition. *Chem Geol* 212:81-100.

Morris JD, Leeman WP, Tera F (1990) The subducted component in island arc lavas: constraints from Be isotopes and B-Be systematics. *Nature* 344:31-36.

Mottl MJ, Wheat G, Fryer P, Gharib J, Martin JB (2004) Chemistry of springs across the Mariana forearc shows progressive devolatilization of the subducting slab. *Geochim Cosmochim Acta* 68:4915-4933.

Münker C, Wörner G, Yogodzinski G., Churikova T (2004) Behaviour of high field strength elements in subduction zones: constraints from Kamchatka-Aleutian arc lavas. *Earth Planet Sci Lett* 224:275-293.

Ohtani E, Toma M, Litasov K, Kubo T, Suzuki A (2001) Stability of dense hydrous magnesium silicate phases and water storage capacity in the transition zone and lower mantle. *Physics of the Earth and Planetary Interiors* 124:105-117.

Pabst, S., Zack, T., Savov, I. P., Ludwig, T., Rost, D., Vicenzi, E. P. (2011) Evidence for boron incorporation into the serpentine crystal structure. *Am Mineral* 96:1112-1119.

Parai, R. I. T. A., and Mukhopadhyay, S. U. J. O. Y. (2012). How large is the subducted water flux? New constraints on mantle regassing rates. *Earth and Planetary Science Letters*, *317*, 396-406.

JA, Peate DW (1995) Tectonic implications of the composition of volcanic arc magmas. *Annu Rev Earth Planet Sci* 23:251-285.

Pearson DG, Brenker FE, Nestola F, McNeill J, Nasdala L, Hutchison MT, Matveev K, Silversmit G, Schmitz B, Vekemans, B, Vincze L (2014). Hydrous mantle transition zone indicated by ringwoodite included within diamond. *Nature*, *507*:221-224.

Peyton V, Levin V, Park J, Brandon M, Lees J, Gordeev E, Ozerov A (2001) Mantle flow at a slab edge: Seismic anisotropy in the Kamchatka region. *Geophys Res Lett* 28:379-382.

Plank, T., and Langmuir, C. H. (1998). The chemical composition of subducting sediment and its consequences for the crust and mantle. *Chemical geology*, *145*(3), 325-394.

Plank T, Cooper LB, Manning CE (2009) Emerging geothermometers for estimating slab surface temperatures. *Nat Geosci* 2:611-615.

Portnyagin, M., Hoernle, K., Avdeiko, G., Hauff, F., Werner, R., Bindeman, I., Garbe-Schönberg, D. (2005) Transition from arc to oceanic magmatism at the Kamchatka-Aleutian junction. *Geology* 33:25-28.

Portnyagin M, Hoernle K, Plechov P, Mironov N, Khubunaya S (2007) Constraints on mantle melting and composition and nature of slab components in volcanic arcs from volatiles (H_2O, S, Cl, F) and trace elements in melt inclusions from the Kamchatka Arc. *Earth Planet Sci Lett* 255:53-69.

Portnyagin M, Manea VC (2008) Mantle temperature control on composition of arc magmas along the Central Kamchatka Depression. *Geology* 36:519-522.

Ranero CR, Phipps Morgan J, McIntosh K, Reichert C (2003) Bending-related faulting and mantle serpentinization at the Middle American trench. *Nature* 425:367-373.

Rosner M, Erzinger J, Franz G, Trumbull RB (2003) Slab-derived boron isotope signatures in arc volcanic rocks from the Central Andes and evidence for boron isotope fractionation during progressive slab dehydration. *Geochem Geophys Geosyst* 4 (9005): 10.1029/2002GC000438.

Rüpke L, Phipps Morgan J, Dixon J (2006) Implications of subduction rehydration for Earth's deep water cycle. *Geophys Monogr Ser* 168:263-276.

Rüpke, L. H., Morgan, J. P., Hort, M., and Connolly, J. A. (2002). Are the regional variations in Central American arc lavas due to differing basaltic versus peridotitic slab sources of fluids?. *Geology*, *30*(11), 1035-1038.

Rüpke, L. H., Morgan, J. P., Hort, M., and Connolly, J. A. (2004). Serpentine and the subduction zone water cycle. *Earth and Planetary Science Letters*, *223*(1), 17-34.

Ryan JG, Langmuir CH (1993) The systematics of boron abundances in young volcanic rocks. *Geochim Cosmochim Acta* 57:1489-1498.

Ryan JG, Morris J, Tera F, Leeman WP, Tsvetkov A (1995) Cross-Arc geochemical variations in the Kurile Arc as a function of slab depth. *Science* 270:625-627.

Savov IP, Ryan JG, D'Antonio M, Fryer P (2007) Shallow slab fluid release across and along the Mariana arc-basin system: Insights from geochemistry of serpentinized peridotites from the Mariana fore arc. *J Geophys Res* 112 (B09205) 10.1029/2006JB004749.

Scambelluri, M., Bottazzi, P., Trommsdorff, V., Vannucci, R., Hermann, J., Gòmez-Pugnaire, M. T., Lòpez-Sànchez Vizcaìno, V. (2001) Incompatible element-rich fluids released by antigorite breakdown in deeply subducted mantle. *Earth Planet Sci Lett* 192: 457-470.

Scambelluri M, Tonarini S (2012) Boron isotope evidence for shallow fluid transfer across subduction zones by serpentinized mantle. *Geology* 40:907-910.

Schellart WP, Jessell MW, Lister GS (2003) Asymmetric deformation in the backarc region of the Kurile arc, northwest Pacific: New insights from analogue modeling. *Tectonics* 22: DOI: 10.1029/2002TC001473.

Smyth JR, Frost DJ, Nestola F, Holl CM, Bromiley (2006) Olivine hydration in the deep upper mantle: Effects of temperature and silica activity. *Geophys. Res. Lett.* 33 (15), DOI: 10.1029/2006GL026194.

Spivack AJ, Edmond JM (1987) Boron isotope exchange between seawater and the oceanic crust. *Geochim Cosmochim Acta* 51:1033-1043.

Stern RJ (2008) Modern-style plate tectonics began in Neoproterozoic time: An alternative interpretation of Earth's tectonic history. *Geological Society of America Special Papers 440:265-280.*

Straub SM, Layne GD (2002) The systematic of boron isotopes in Izu arc front volcanic rocks. *Earth Planet Sci Lett* 198:25-39.

Tonarini S, Leeman WP, Leat PT (2011) Subduction erosion of forearc mantle wedge implicated in the genesis of the South Sandwich Island (SSI) arc: Evidence from boron isotope systematics. *Earth Planet Sci Lett* 301:275-284.

Ulmer P, Trommsdorff V (1995) Serpentine stability to mantle depths and subduction-related magmatism. *Science* 268:858-861.

van Keken PE, Hacker BR, Syracuse EM, Abers GA (2011) Subduction factory: 4. Depth-dependent flux of H_2O from subducting slabs worldwide. *J Geophys Res* 116 (B01401): 10.1029/2010JB007922.

Vils F, Pelletier L, Kalt A, Müntener O, Ludwig T (2008) The lithium, boron and beryllium content of serpentinized peridotites from ODP leg 209 (sites 1272A and 1274A): Implications for lithium and boron budgets of oceanic lithosphere. *Geochim Cosmochim Acta* 72:5475-5504.

Walowski KJ, Wallace PJ, Hauri EH, Wada I, Clynne MA (2015) Slab melting beneath the Cascade Arc driven by dehydration of altered oceanic peridotite. Nat. Geosci. 8:404-409.

Wunder B, Meixner A, Romer RL, Wirth R, Heinrich W (2005) The geochemical cycle of boron: Constraints from boron isotope partitioning experiments between mica and fluid. *Lithos* 84:205-216.

Workman, R. K., and Hart, S. R. (2005). Major and trace element composition of the depleted MORB mantle (DMM). *Earth and Planetary Science Letters*, *231*(1), 53-72.

Yogodzinski, G. M., Lees, J. M., Churikova, T. G., Dorendorf, F., Wöerner, G., Volynets, O. N. (2001) Geochemical evidence for the melting of subducting oceanic lithosphere at plate edges. Nature 409:500-504.

Figure Legends

Figure 1: (A) Topographic map (SRTM) and geological structures of the Kamchatka subduction zone. The inset shows the three volcanic chains and the extent of the Central Kamchatkan Depression (CKD). The stippled lines in the main map are isolines for the slab surface depth and the numbers indicate the depth (data from Gorbatov et al., 1997). Circles indicate volcanic centers. (B) The upper panel shows the relation between slab surface depth and B geochemistry in the arc volcanic rocks. Circles are $\delta^{11}B$ values and triangles mark B/Nb. As there is a significant along-arc extent of the data points, filled symbols indicate values in the volcanoes that are nearest to the profile. The middle panel shows the digital elevation model (ASTER) and the lowermost panel the modeled thermal patterns used for the thermodynamic calculations.

Figure 2: Correlation of Ba/Nb, Th/Nb and Ba/Th with slab depth in the Kamchatkan arc. Ba/Nb and Ba/Th are constant or slightly decreasing with increasing slab depth in the EVF and strongly increasing in the CKD lavas. Th/Nb is (with one outlier) constant throughout both chains. Data are compiled from Churikova et al., 2001, Portnyagin et al., 2007 and Duggen et al., 2007.

Figure 3: Modeled dehydration in all three profiles in models with 2.5wt% water in the uppermost 15km of the slab slab mantle. The upper panel shows the water release at the top of the model color-coded for the source of the fluid. Light blue: wedge mantle, red: sediments and AOC, dark blue: slab mantle. High frequency variations are due to the incrementation of the model. The middle panel shows the DEM (ASTER) and the lower panel illustrates the distribution of free water within the slab together with the dehydration reactions. In the northern and central profiles slab mantle dehydration starts at the deepest hydrated part followed by dehydration in the uppermost slab mantle. In the lower part the liberated water is absorbed in the overlying water under-saturated part and released not before the tip of the atg-out reaction. In the southern profile low intra-slab temperatures allow an entire water transfer into Phase A without water liberation. See text for further details.

Figure 4: Release of boron and corresponding $\delta^{11}B_{fluid}$ values in the models shown in Fig. 3. Uppermost panel: Relation between amount of water released at the top of the model, the B concentration therein and the amount of B released from the slab. The comparison shows that the B release is predominantly controlled by the fluid amount rather than by the B concentration in the fluid. Second panel: $\delta^{11}B_{fluid}$ values in the released water. Extremely high $\delta^{11}B_{fluid}$ values characterize water release into the forearc in all models. Across the EVF, $\delta^{11}B_{fluid}$ values systematically decrease, reflecting continuous dehydration. The increase in $\delta^{11}B_{fluid}$ values at the CKD is coupled to serpentine dehydration in the slab mantle. Different $\delta^{11}B_{fluid}$ curves in the northern profile result from different water contents in the slab mantle. Third panel: DEM data. Lowermost panel: $\delta^{11}B_{fluid}$ values within the free fluid phase in the three slabs. Note the

high $\delta^{11}B_{fluid}$ values released by serpentine breakdown in the slab mantle enriching the oceanic crust and the wedge mantle in ^{11}B.

Figure 5: Water content of the slab and subduction of water beyond sub-arc depth. The right column shows the water content of the slab assuming 2.5 wt% water in the slab mantle. The left column shows the water distribution in the slab along a vertical cross section at the largest slab depth. In all profiles wedge mantle and MORB do not contribute significant amounts of water beyond subarc depths. In contrast, phengite (in sediments) and phase A (in the slab mantle) remain as stable hydrous phases and are able to transport water into the deep mantle. In all profiles beyond arc water fluxes are constrained by the thermal stability of phase A, but in the northern and central profiles 2.5 wt% water within 15 km slab mantle are sufficient to saturate the beyond arc slab mantle. See text for further discussion.

Figure 6: The sigmoidal curve shows the relationship between beyond-arc water flux, hydration depth and initial water content of the slab mantle in the northernmost profile. The bold italic numbers show the minimum amount of water necessary to fully hydrate the slab mantle beyond arc (bell-shaped curve in Fig. 5). The circles and italic numbers show the slab mantle water content of those model runs that reproduce the B pattern in the arc lavas.

Figure 7: Comparison of the results of this study with published datasets for beyond-arc water fluxes. Shown are the results from Hacker 2008 and Van Keken et al., 2011,

published on Kamchatka data as well as global estimates for beyond arc water subduction.

Figure 8: Variation of the critical parameters. The diagrams show the effect of the variation of the most critical input parameters (B concentration, initial $\delta^{11}B$ as well as the lawsonite-fluid distribution coefficient for B) on the resulting $\delta^{11}B$ pattern. The green curves indicate the results shown in the paper, other curves are labeled for the parameter variations.

Table 1: Calculated beyond-arc water fluxes from the models shown in Fig. 5

Figure 1

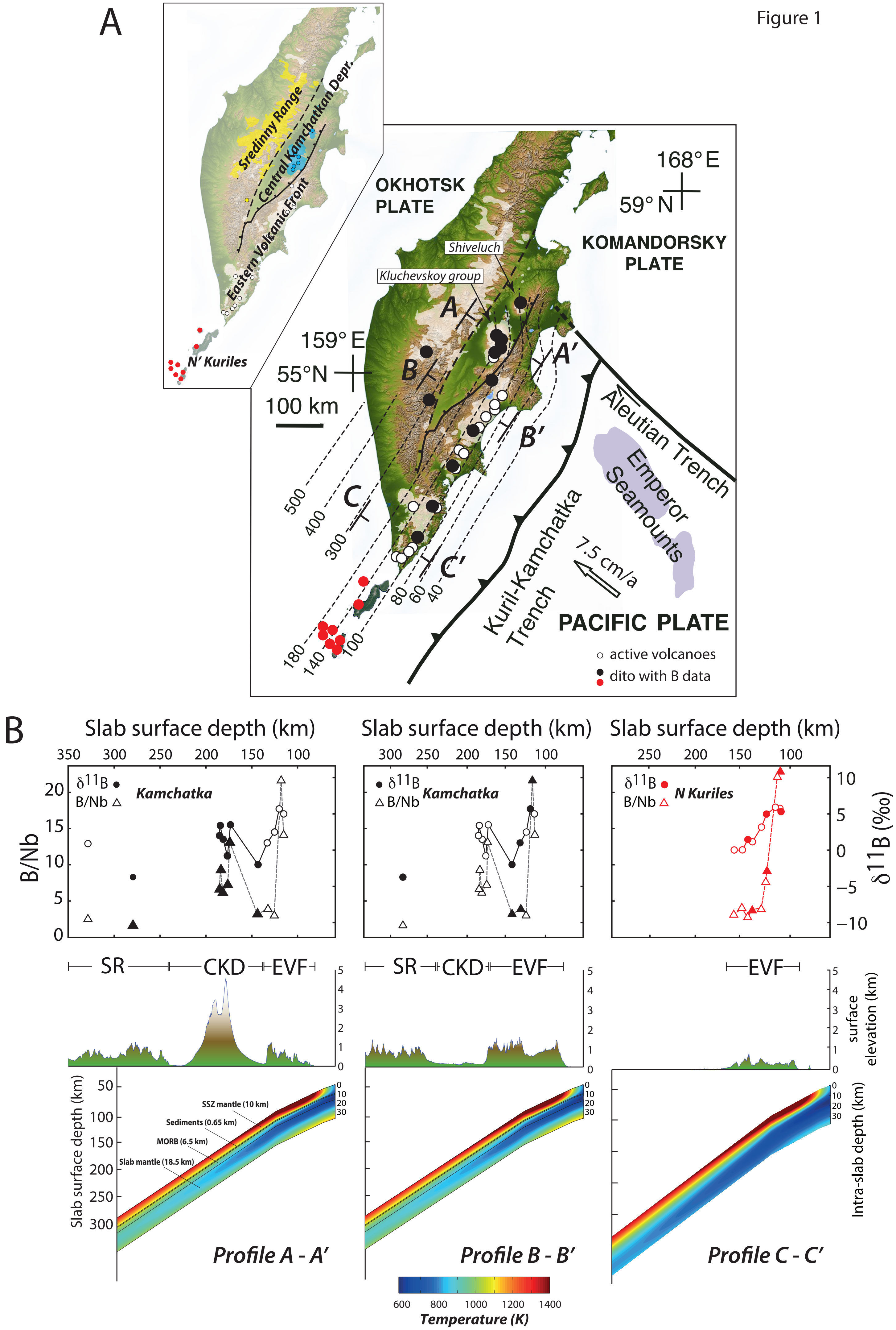
A
Sredinny Range
Central Kamchatkan Depr.
Eastern Volcanic Front
N' Kuriles
OKHOTSK PLATE
168° E
59° N
KOMANDORSKY PLATE
Shiveluch
Kluchevskoy group
159° E
55°N
100 km
Aleutian Trench
Emperor Seamounts
Kuril-Kamchatka Trench
7.5 cm/a
PACIFIC PLATE
active volcanoes
dito with B data
B
Slab surface depth (km)
B/Nb
δ11B (‰)
Kamchatka
N Kuriles
SR
CKD
EVF
surface elevation (km)
Slab surface depth (km)
Intra-slab depth (km)
SSZ mantle (10 km)
Sediments (0.65 km)
MORB (6.5 km)
Slab mantle (18.5 km)
Profile A - A'
Profile B - B'
Profile C - C'
Temperature (K)

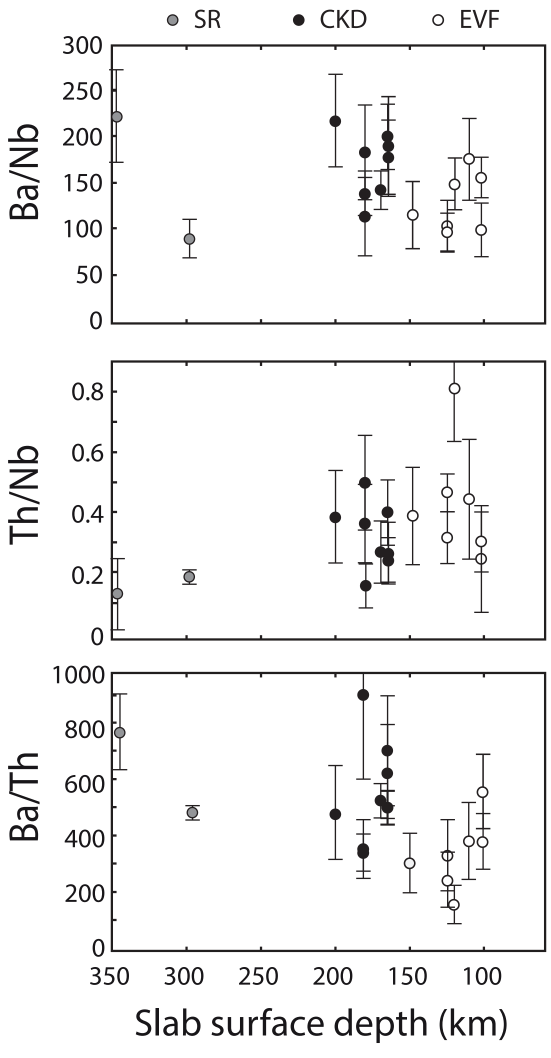

SR
CKD
EVF
Ba/Nb
Th/Nb
Ba/Th
Slab surface depth (km)

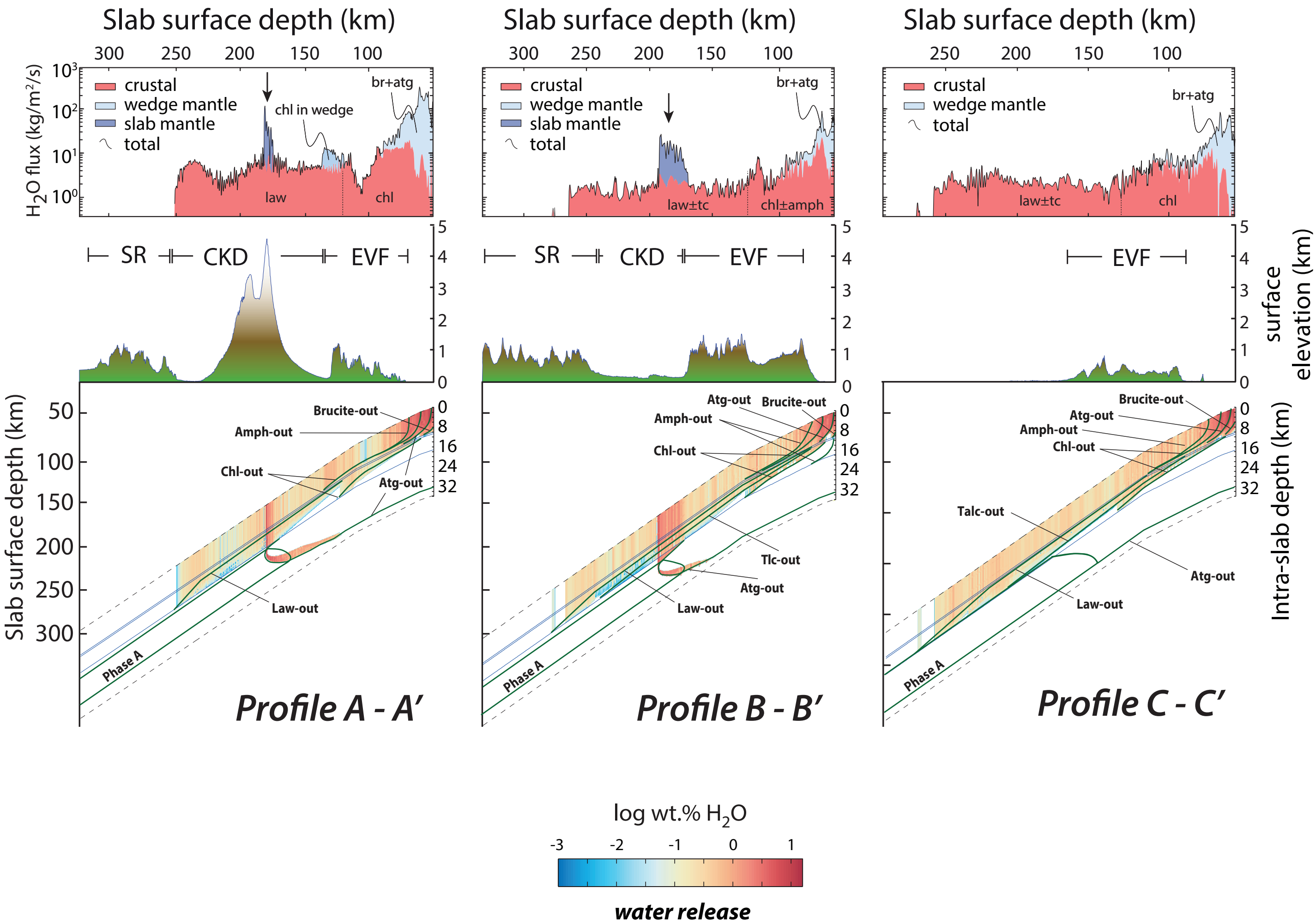

Slab surface depth (km)
H2O flux (kg/m²/s)
crustal
wedge mantle
slab mantle
total
chl in wedge
br+atg
law
chl
law±tc
chl±amph
SR
CKD
EVF
surface elevation (km)
Slab surface depth (km)
Intra-slab depth (km)
Brucite-out
Amph-out
Chl-out
Atg-out
Law-out
Tlc-out
Talc-out
Phase A
Profile A - A′
Profile B - B′
Profile C - C′
log wt.% H2O
water release

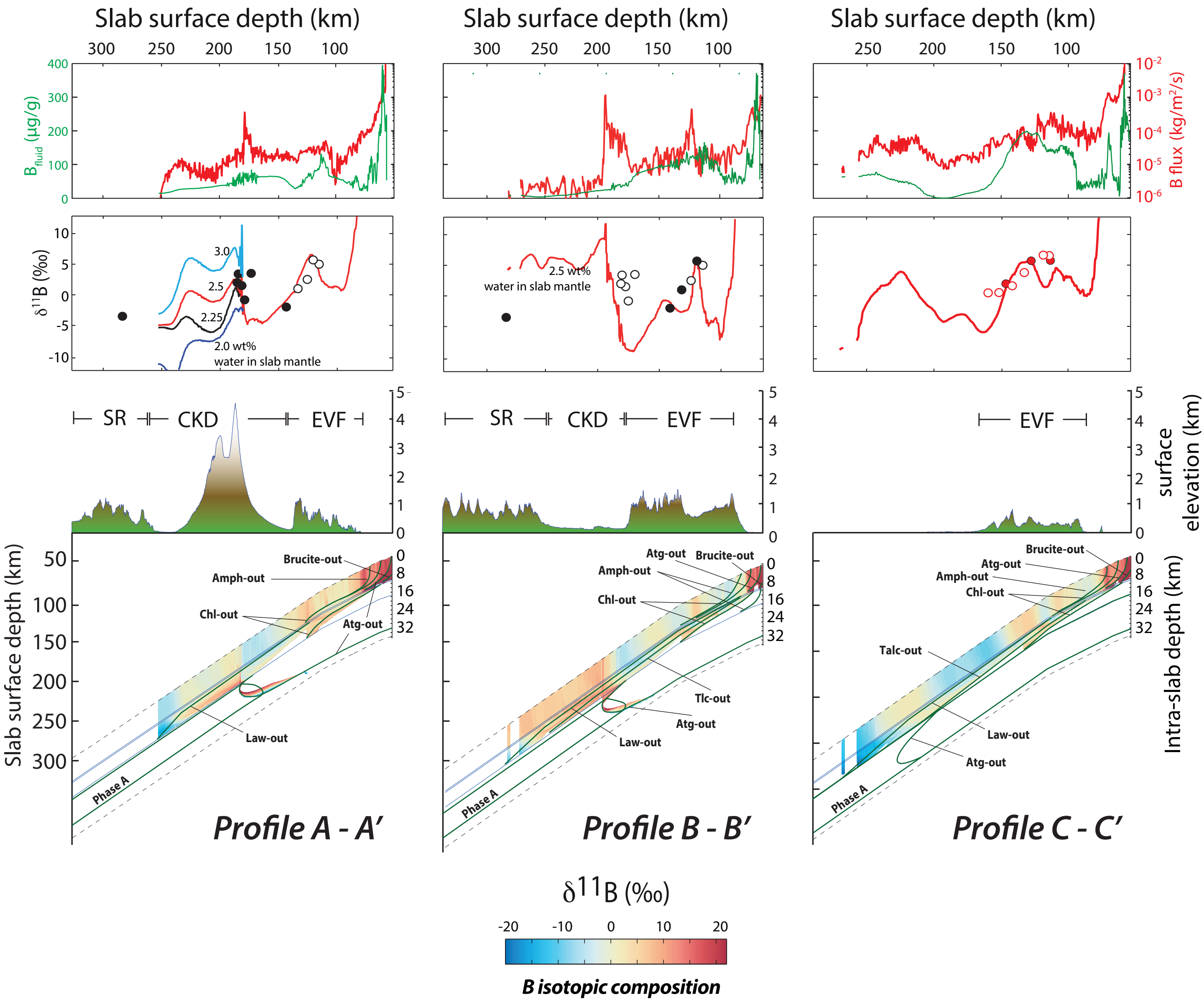

Slab surface depth (km)
Slab surface depth (km)
Slab surface depth (km)
B_fluid (μg/g)
B flux (kg/m²/s)
δ11B (‰)
3.0
2.5
2.25
2.0 wt%
water in slab mantle
2.5 wt%
water in slab mantle
SR
CKD
EVF
surface elevation (km)
Brucite-out
Amph-out
Chl-out
Atg-out
Law-out
Tlc-out
Talc-out
Phase A
Intra-slab depth (km)
Profile A - A′
Profile B - B′
Profile C - C′
δ11B (‰)
B isotopic composition

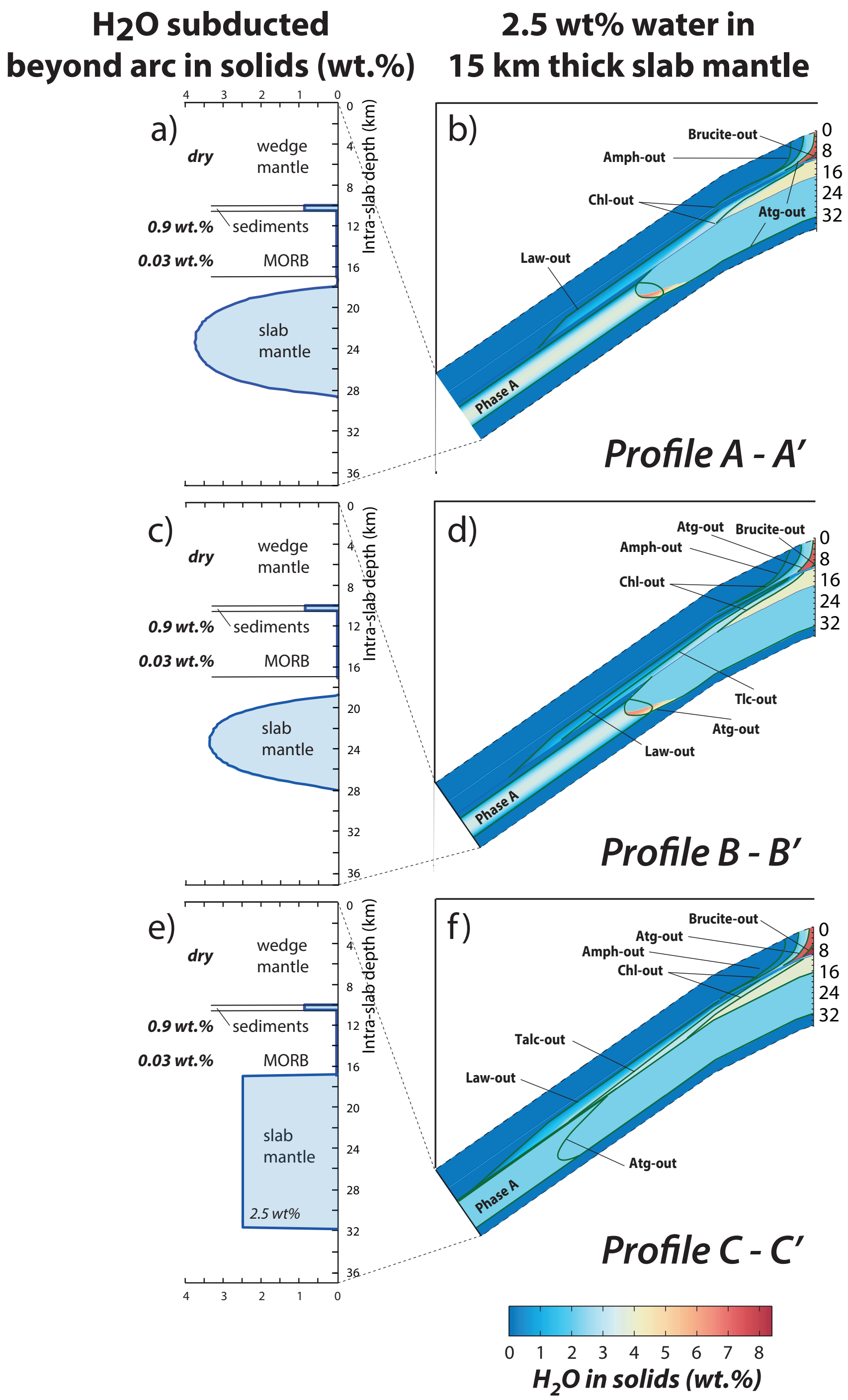
H2O subducted
beyond arc in solids (wt.%)
2.5 wt% water in
15 km thick slab mantle
a)
dry
wedge mantle
0.9 wt.%
sediments
0.03 wt.%
MORB
slab mantle
Intra-slab depth (km)
b)
Brucite-out
Amph-out
Chl-out
Atg-out
Law-out
Phase A
Profile A - A'
c)
d)
Atg-out
Brucite-out
Amph-out
Chl-out
Tlc-out
Atg-out
Law-out
Profile B - B'
e)
2.5 wt%
f)
Brucite-out
Atg-out
Amph-out
Chl-out
Talc-out
Law-out
Atg-out
Profile C - C'
H2O in solids (wt.%)

Figure 4

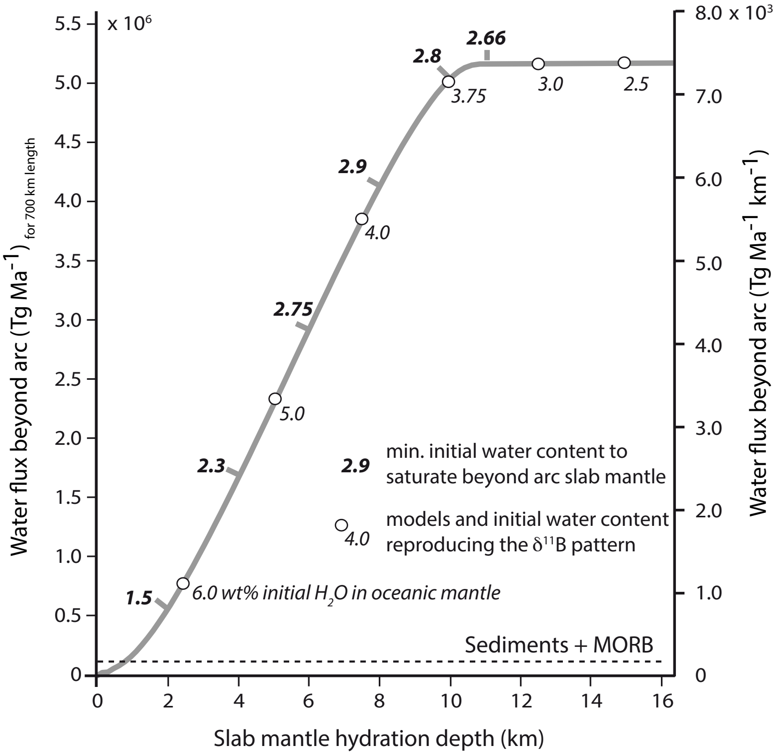
x 10⁶
8.0 x 10³
Water flux beyond arc (Tg Ma⁻¹) for 700 km length
Water flux beyond arc (Tg Ma⁻¹ km⁻¹)
Slab mantle hydration depth (km)
2.9 min. initial water content to saturate beyond arc slab mantle
4.0 models and initial water content reproducing the δ¹¹B pattern
6.0 wt% initial H₂O in oceanic mantle
Sediments + MORB

Figure 5

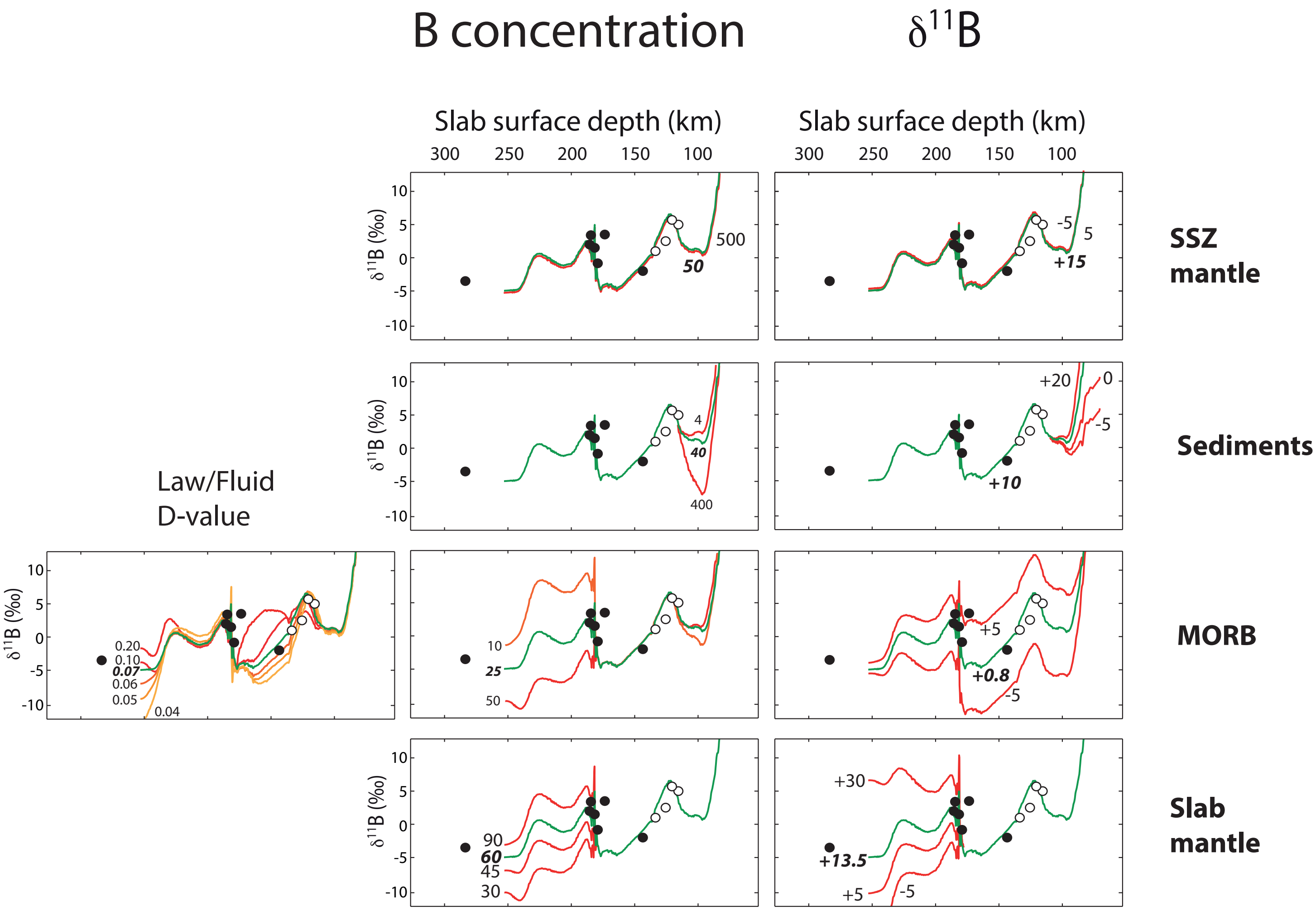

B concentration
δ^{11}B
Slab surface depth (km)
300 250 200 150 100
δ^{11}B (‰)
SSZ mantle
Sediments
MORB
Slab mantle
Law/Fluid D-value
500
50
-5
5
+15
4
40
400
+20
0
+10
10
25
+5
+0.8
90
60
45
30
+30
+13.5
+5
0.20
0.10
0.07
0.06
0.05
0.04

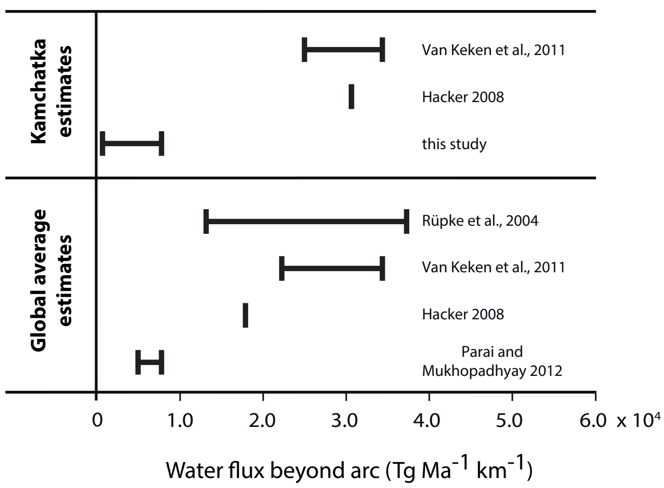
Kamchatka estimates
Global average estimates
Van Keken et al., 2011
Hacker 2008
this study
Rüpke et al., 2004
Van Keken et al., 2011
Hacker 2008
Parai and Mukhopadhyay 2012
0
1.0
2.0
3.0
4.0
5.0
6.0
x 10⁴
Water flux beyond arc (Tg Ma-1 km-1)

Figure 7

2.5 wt% water in uppermost15 km slab mantle

	Average water content in hydrated part beyond arc:	Deep water recycling rate at 7.5 cm/a convergence	
Profile A - A′	***2.86 wt.%***	***7.5 x10^{3} Tg/Ma/km***	*Fig. 4b*
Profile B - B′	***2.53 wt.%***	***6.5 x10^{3} Tg/Ma/km***	*Fig. 4d*
Profile C - C′	***2.5 wt.%***	***9.5 x10^{3} Tg/Ma/km***	*Fig. 4f*
Kamchatka average	***2.63 wt.%***	***7.8 x 10^{3} Tg/Ma/km*** over 700km: ***5.5 x 10^{6} Tg/Ma***	

Appendix to Konrad-Schmolke, M., Halama, R. and Manea, V. 2016:

"Slab mantle dehydrates beneath Kamchatka – yet recycles water into the deeper mantle"

General model approach

The numerical model that we use is a combination of thermomechanical, thermodynamic and mass balanced trace element calculations. Modeling consists of the following four steps: (1) A thermal pattern of the Kamchatkan subduction zone is modeled, utilizing a finite element thermomechanical code, and discretized (Manea and Manea, 2007), (2) the discretized pressure-temperature-distance relations derived from the thermomechanical model are used as input for a Gibbs energy minimization algorithm that simulates the passing of a vertical rock column within the subducted slab (Connolly 2005) through the modeled steady state thermal pattern. Based on the modeled pressure-temperature relations, phase relations are calculated at every discretized increment with a resolution of 250 x 250m. Water liberated by dehydration reactions is transported vertically upward equilibrating at every calculated increment within the column and thus reflecting a high ratio of fluid/slab migration velocity. (3) The modeled phase relations at every calculated increment are used for a coefficient-based mass-balanced boron distribution among the stable solid and liquid phases. (4) A temperature-dependent fluid-solid boron isotope fractionation based on experimentally determined functions (Wunder et al., 2005) is calculated to determine the amounts of ^{10}B and ^{11}B in solids and fluid. Boron incorporated into the fluid phase is assumed to migrate upward into the next calculated increment and re-distributed. Elements retained in the solids are transported within the slab and form the initial bulk rock composition in the next rock column. Therefore the model simulates fluid release, fluid migration, boron transport and boron isotope fractionation in a subducted slab passing through a steady state thermal pattern.

Thermomechanical model

The steady-state thermomechanical models of Manea and Manea (2007) consist of five thermo-stratigraphic units: the upper and lower continental crust, the oceanic lithosphere and sediments, and the mantle wedge. The boundary conditions employed in these numeric models are as following: the upper and lower boundaries correspond to 0°C and 1450°C respectively, the left (landward) boundary is defined by a 22.5°C/km thermal gradient for the continental crust, and 10°C/km for the lithospheric mantle, and the right (oceanic) boundary is age dependent corresponding to an oceanic geotherm calculated using GDH1 model of Stein and Stein (1992). Although advanced 3D numeric models of subduction zone would have been preferable, the depth, thickness and geometry of different layers used in the 2D steady-state thermomechanical models of Manea and Manea (2007) are well constrained by seismological data. Also, the oceanic boundary conditions, that strongly control the slab thermal structure, are in good agreement with the age of the incoming Pacific plate. Although there is seismological evidence of slab breaking beneath the northern part of Kamchatka in the last 10 Ma (Levin et al., 2002), a process that potentially would have triggered mantle upwelling in that region, there are no currently published well-constrained 3D thermomechanical models that take into account the long-term geodynamical evolution of the entire Kamchatka subduction system.

Thermodynamic model

The thermodynamic model approach used in this work was first published by Connolly (2005). The steady state thermal pattern of the slab is divided into P-T increments at each of which the Gibbs energy among the database phases is minimized and the stable assemblage as well as the composition of the coexisting phases is determined (Fig. A1). A list of the solid solution models used in the calculations is given in Table A1. The modeled slab consists of four lithologically different layers: a 10 km thick wedge mantle layer that has primitive upper mantle composition (Workman and Hart, 2005), a 0.65 km thick sediment layer (N Pacific sediment; Plank and Langmuir, 1998), a 6.5 km thick MORB-type oceanic crust (Workman and Hart, 2005) and a 18.5 km thick layer with depleted mantle composition (Workman and Hart, 2005) (Fig. A2).

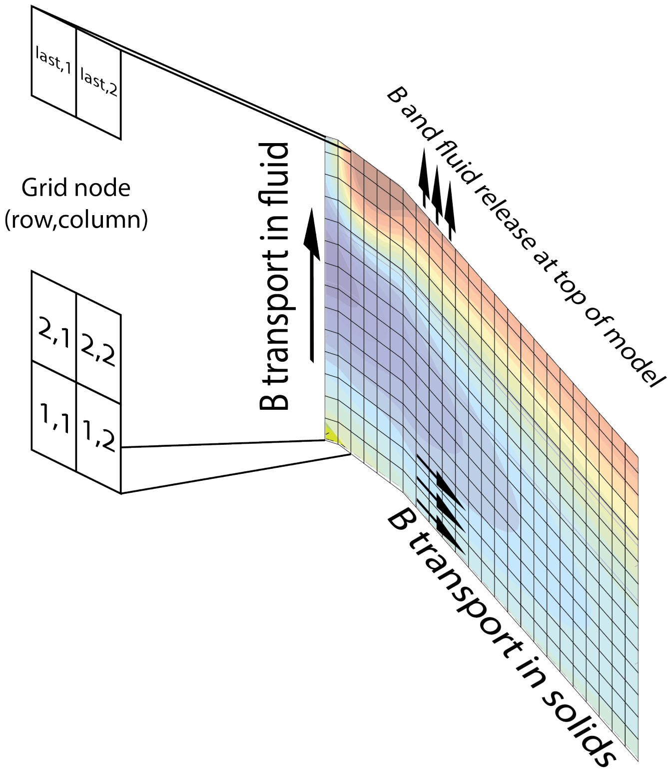

Fig. A1: The thermal pattern is discretized into 221 x 997 grid nodes at each of which Gibbs energy minimization is performed. The spatial resolution of the model is 250x250 m. Free water (and boron therein) is transferred into the overlying grid node within a column. Major elements and boron in solids are transferred into the next column.

To model the migration of the slab through the steady state thermal pattern and the resulting fluid migration, our calculations start at the lowermost increment of the slab at the beginning of subduction. Amounts and compositions of stable phases are determined and the modeled amount of the free fluid phase is transferred to the next overlying P-T increment. Here, phase assemblage and composition are modeled taking into account the fluid added from below. At the uppermost increment the fluid is assumed to leave the model. The next modeled column starts again at the lowermost increment with the bulk rock composition being determined as the composition of the same increment in the afore-calculated column minus the amount of elements that were transferred upward in the migrating fluid.

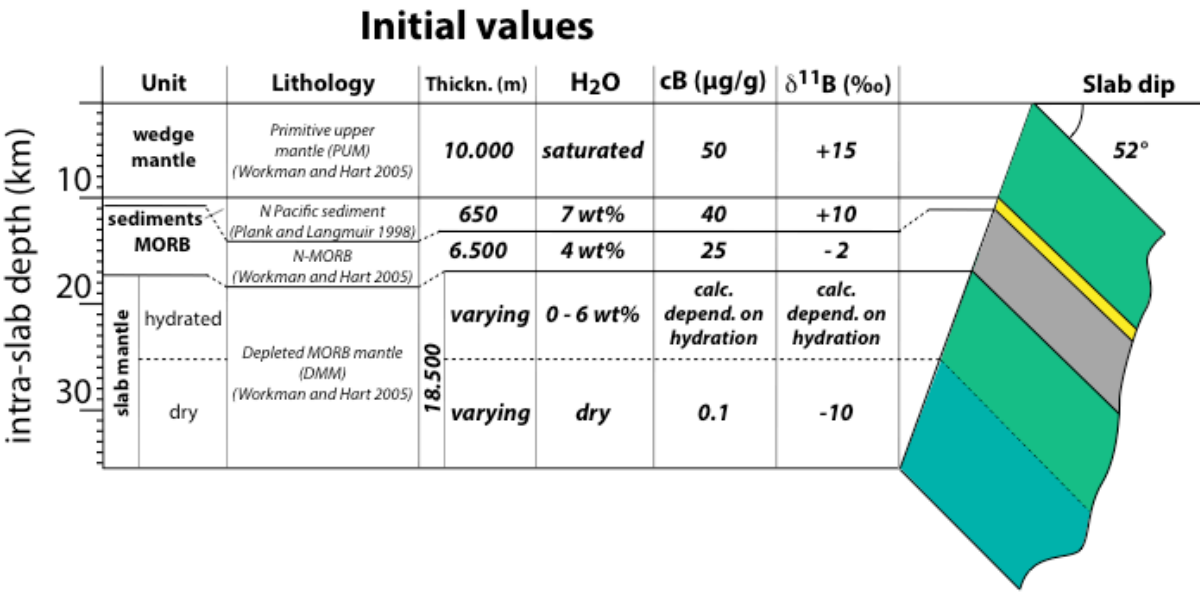

Fig. A2: Composition of the layered slab and initial input values.

Chemical input parameters

The initial water distribution in the slab assumes water saturation in the sediment and the MORB layer. Water saturation in the 10 km thick mantle wedge layer is the result of initial dehydration of the oceanic crust in the first calculated model column. The boron concentrations in the wedge mantle, the sediments and the MORB layers are 50, 40 and 25 µg/g respectively (Spivack and Edmond 1987; Ishikawa and Nakamura 1993; Smith et al., 1995). The initial $\delta^{11}B_{(Bulk)}$ of the sediment and MORB layers is assumed to be +5‰ and -2‰ (Spivack and Edmond 1987). The initial $\delta^{11}B_{(Bulk)}$ in the slab mantle layer is calculated by the amount of serpentine initially present under the hydration state at the onset of subduction. A boron concentration of 60 µg/g in serpentine, an initial $\delta^{11}B_{(Serpentine)}$ of +13.5‰ (Boschi et al., 2008) as well as a boron concentration of 0.1µg/g and a $\delta^{11}B$ of -10‰ in dry peridotite is assumed. During forward modeling changing $\delta^{11}B_{(Bulk)}$ is calculated by fractionating ^{10}B and ^{11}B into the migrating fluid according to the modeled $\Delta^{11}B_{(Mineral\text{-}Fluid)}$ (Fig. A4).

Boron distribution calculation

Under the assumption of thermodynamically independent trace element incorporation into stable phases it is possible to calculate trace element concentrations in coexisting phases by distributing a given amount of elements present in the bulk rock or effective (i.e. reacting) bulk rock volume according to bulk distribution coefficients among the thermodynamically modeled stable phases. The fluid-solid boron distribution is done by calculating a Fluid/Matrix distribution coefficient ($D_B^{Fluid/Matrix}$) at each calculated increment, where

$$D_B^{Fluid/Matrix} = \sum_{k=1} D_B^{(Fluid/Mineral)_k} \cdot X_{Mineral_k}$$

with k denoting the stable minerals present at each calculation step and $D_B^{Fluid/Mineral}$ is the B distribution coefficient for the fluid with respect to a certain mineral. A list of distribution coefficients used and their sources are given in Table A1. In order to account for channelized fluid flux and the resulting limited fluid-rock interaction in garnet-pyroxene rocks, i.e. eclogites (e.g., Zack and John 2007), the reacting garnet and pyroxene fractions were reduced to be only 25% of the thermodynamically stable mineral modes.

Based on the bulk distribution coefficient the concentration of boron in the fluid and solids is calculated at each step by

$$C_B^{Fluid} = \frac{C_B^{Bulk}}{(X_{Solids}/(D_B^{Fluid/Matrix} \cdot X_{Fluid})) + 1}$$

Where C_B^{Bulk} is the B concentration in the bulk rock or effective bulk rock volume and X_{Solids} and X_{Fluid} being the weight proportions of the solids and the fluid. Element fractionation effects or fluid mediated element influx is modeled by changing the bulk rock or effective bulk rock composition at every calculated step.

Boron isotope calculations

Boron isotope composition in fluid and solids are calculated at every calculated increment based on the temperature-dependent fractionation function published in Wunder et al., 2005 (Fig. A3):

$$\Delta^{11}B_{(Mineral\text{-}Fluid)} = -10.69\ (1000/T[K]) + 3.88$$

where

$$\Delta^{11}B_{(Mineral\text{-}Fluid)} = \delta^{11}B_{(Mineral)} - \delta^{11}B_{(Fluid)}.$$

Knowing the initial $\delta^{11}B_{(Bulk)}$ at the beginning of the modeling, $\delta^{11}B_{(Solids)}$ and $\delta^{11}B_{(Fluid)}$ can be calculated at each step after boron distribution among the solids and the fluid.

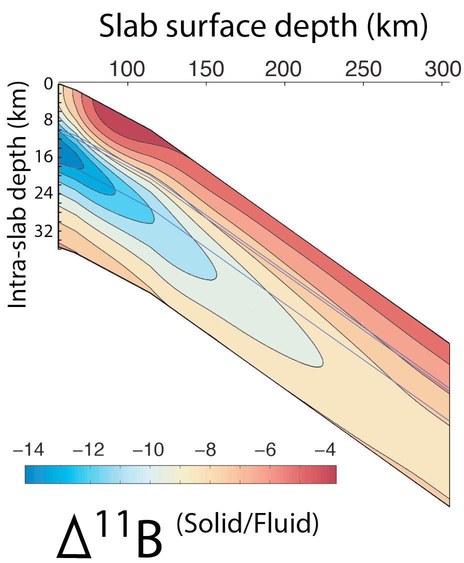

Fig. A3: Modeled temperature dependent solid-fluid boron isotope fractionation calculated after Wunder et al., 2005.

Table A1: $B^{Solid/Fluid}$ partition coefficients

Solid/Fluid pair	**Value**	**Source**
Cpx/Fluid	0.016	Brenan et al., 1998
Grt/Fluid	0.0006	Brenan et al., 1998
Atg/Fluid	0.2	Estimated
Mica/Fluid	0.2	Brenan et al., 1998
Law/Fluid	0.07 (0.04)	Estimated (Brenan et al., 1998)
Amph/Fluid	0.016	Brenan et al., 1998
Chl/Fluid	0.0025	Estimated

Cpx=clinopyroxene, Grt=garnet, Atg=antigorite (serpentine), Law=lawsonite, Amph=amphibole, Chl=chlorite

Table A2: Solid solution formulations used in the thermodynamic calculations

Solid solution	Exchange vectors	Source
Amphibole	$Ca_{2-2w}Na_{z+2w}[Mg_xFe_{1-x}]_{3+2y+z}Al_{3-3y-w}Si_{7+w+y}O_{22}(OH)_2$, w+y+z<=1	[1, 2]
Antigorite	$Mg_{48x}Fe_{48(1-x)}Si_{34}O_{85}(OH)_{62}$	Ideal
Chlorite	$[Mg_xFe_wMn_{1-x-w}]_{5-y+z}Al_{2(1+y-z)}Si_{3-y+z}O_{10}(OH)_8$, x+w<=1	[3]
Clinopyroxene	$Na_{1-y}Ca_yMg_{xy}Fe_{(1-x)y}Al_ySi_2O_6$	[4]
Epidote	$Ca_2Al_{3-2x}Fe_{2x}Si_3O_{12}(OH)$	[5]
Feldspar	$K_yNa_xCa_{1-x-y}Al_{2-x-y}Si_{2+x+y}O_8$, x+y<=1	[6]
Garnet	$Fe_{3x}Ca_{3y}Mg_{3z}Mn_{3(1-x-y-z)}Al_2Si_3O_{12}$, x+y+z<=1	[7]
Olivine	$Mg_{2x}Fe_{2y}Mn_{2(1-x-y)}SiO_4$, x+y<=1	[7]
Orthopyroxene	$[Mg_xFe_{1-x}]_{2-y}Al_{2y}Si_{2-y}O_6$	[4]
Phase A	$Mg_{7x}Fe_{7(1-x)}Si_2O_8(OH)_6$	Ideal
Spinel	$Mg_xFe_{1-x}Al_2O_3$	Ideal
Talc	$[Mg_xFe_{1-x}]_{3-y}Al_{2y}Si_{4-y}O_{10}(OH)_2$	Ideal
White mica	$K_xNa_{1-x}Mg_yFe_zAl_{3-2(y+z)}Si_{3+y+z}O_{10}(OH)_2$	[5]

Flow chart of the modeling procedure

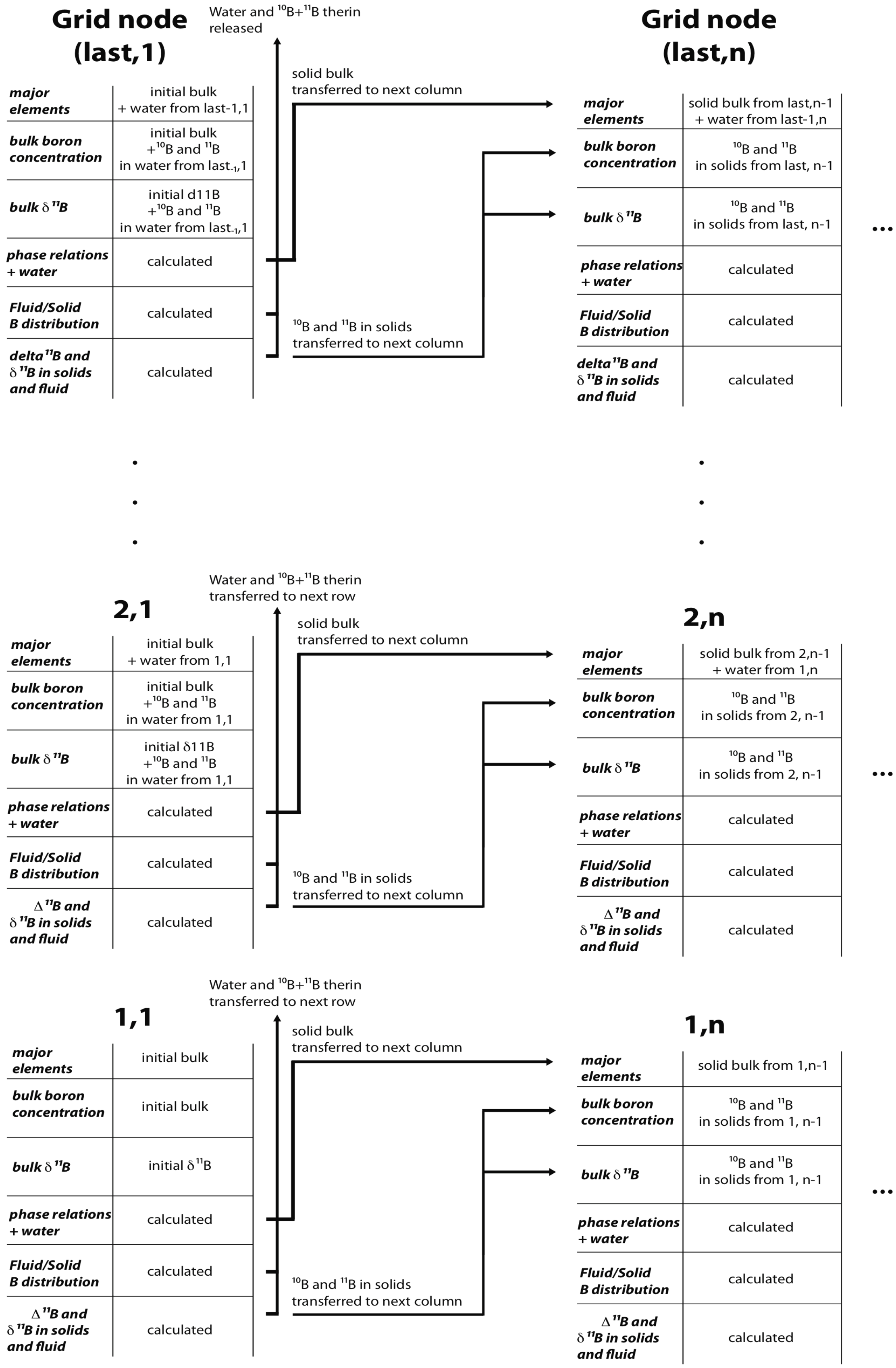

Solid solution source references

1. Wei, C.J. & Powell, R. Phase relations in high-pressure metapelites in the system KFMASH (K_2O-FeO-MgO-Al_2O_3-SiO_2-H_2O) with application to natural rocks. *Contrib. Mineral. Petrol.* **145**, 301-315. (2003).

2. White, R.W., Powell, R. & Phillips, G.N. A mineral equilibria study of the hydrothermal alteration in mafic greenschist facies rocks at Kalgoorlie, Western Australia. *J. Metamorph. Geol.* **21,** 455-468 (2003).

3. Holland, T.J.B., Baker, J. & Powell, R. Mixing properties and activity-composition relationships of chlorites in the system MgO- FeO- Al_2O_3-SiO_2-H_2O. *Europ. J. Mineral.* **10**, 395-406 (1998).

4. Holland, T. & Powell, R. Thermodynamics of order-disorder in minerals. Symmetric formalism applied to solid solutions. *Am. Mineral.* **81**, 1425-1437 (1996).

5. THERMOCALC datasets: http://www.metamorph.geo.uni-mainz.de/thermocalc/datafiles/index.html

6. Fuhrman, M.L. & Lindsley, D.H. Ternary-Feldspar Modeling and Thermometry. *Am. Mineral.* **73**, 201-215 (1988).

7. Holland, T.J.B. & Powell, R. An internally consistent thermodynamic data set for phases of petrological interest. *J. Metamorph. Geol.* **16**, 309-343 (1998).